WILEY-VCH

DOI: 10.1002/((please add manuscript number))
Article type: Progress Report

Towards Efficient Spectral Converters through Materials Design for Luminescent Solar Devices

*Barry McKenna and Rachel C. Evans**

Barry McKenna and Dr. Rachel C. Evans
School of Chemistry & CRANN, Trinity College Dublin, Dublin 2, Ireland
E-mail: raevans@tcd.ie

Dr Rachel C. Evans
Department of Materials Science & Metallurgy, University of Cambridge, 27 Charles Babbage Road, Cambridge, CB3 0FS, U.K.

Keywords: luminescence, downshifting, solar concentrator, upconversion, solar energy, photovoltaic device, triplet-triplet annihilation

Abstract

Single junction photovoltaic devices exhibit a bottleneck in their efficiency due to incomplete or inefficient harvesting of photons in the low- or high-energy regions of the solar spectrum. Spectral converters can be used to convert solar photons into energies that are more effectively captured by the photovoltaic device through a photoluminescence process. In this progress report, recent advances in the fields of luminescence solar concentration, luminescence downshifting and upconversion are discussed. Our focus is specifically on the role that materials science has to play in overcoming barriers in the optical performance in all spectral converters and on their successful integration with both established (e.g. c-Si, GaAs) and emerging (perovskite, organic, dye-sensitized) cell types. Current challenges and emerging research directions, which need to be addressed for the development of next-generation luminescent solar devices, are also discussed.

1. Introduction

Solving the global energy crisis is without doubt one of the most important scientific challenges facing mankind. New technologies that effectively harness renewable energy sources, such as

the sun, wind and tides, are acknowledged to be the most viable long-term solution. Solar energy, in particular, has long been considered an attractive prospect due to the abundance of sunlight arriving at the Earth's surface. However, a major bottleneck limiting the efficiency of all commercialized and emerging photovoltaic (PV) technologies is the inability to effectively harvest all wavelengths of light available in the solar spectrum.[1] For single junction crystalline silicon (c-Si) PV cells, the Shockley-Queisser limit shows that the conversion efficiency is capped at ~30%.[2]The photogeneration of charge carriers only occurs if the device absorbs solar photons with energies corresponding to that of the band gap energy (E_g) or greater. All photons of energy less than E_g falling on the PV cell will be transmitted through the device and lost. However, the absorption of photons greater than E_g is also inefficient, with the excess energy gained being lost as heat through non-radiative recombination of the photoexcited charge carriers. Intrinsic spectral losses thus represent a major efficiency shortfall in PV cells.

Spectral converters show huge potential for integration with solar cells to overcome fundamental non-absorption and thermalization losses.[3] They are applied to a finished solar cell in the form of an active photoluminescent layer, whose role is to absorb solar photons that cannot be captured effectively and convert them to wavelengths more suitable for use. Spectral converters offer the advantage of not requiring modifications to the standard solar cell architecture or the intrinsic device materials, and allow for facile optimization towards a specific type of solar cell through judicious selection of the luminophore used. Moreover, space requirements, coupled with reduced performance in diffuse sunlight conditions, mean that arrays of conventional solar panels may not be the most cost-effective nor practical solution in built-up areas. Spectral converters may help overcome some of these limitations, with the application of colorful photoluminescent films to any available surface (*e.g.* façades, roofs, windows, walls *etc*…) coupled to highly efficient, smaller PV cells enabling the transformation of everyday buildings into solar harvesting machines.

In this progress report, recent developments in the application of solar converters to improve the efficiency of PV devices are discussed. Two methods based on photoluminescence are considered in detail: luminescence down-shifting (DS), in both layer and concentrator architectures, and upconversion (UC). The fundamental theories underpinning each process are well-established, and there are several in-depth reviews summarizing the key requirements and properties of the most commonly used luminophores for each spectral conversion mechanism.[3–6] Our specific focus here is to show how materials science can contribute to the development of more efficient spectral converters, for example through the chemical design of functional and/or hierarchically-structured host materials which enable tuning of the luminescence properties, or novel materials engineering approaches to improve integration with PV devices. We begin with a summary of the spectral requirements for different PV devices, the physical principles of spectral conversion and the different architectures used to integrate the spectral conversion layer. Each spectral conversion mode is then considered in detail in terms of the fundamental materials' requirements and key examples from the recent literature that have driven a paradigm shift in the direction of the field are presented. Particular attention will be paid to the integration of spectral converters with emerging PV technologies such as perovskite and organic solar cells. Finally, a brief perspective about the remaining challenges and future prospects in the field of spectral converters is presented.

2. Which Spectral Converter for Which Photovoltaic Device?

The spectral distribution of sunlight at Air Mass 1.5 global (AM 1.5 G) consists of photons with wavelengths spanning the ultraviolet (UV) to infrared (280 – 2500 nm, 0.5-4.4 eV) region. The spectral response of a PV cell is described by its external quantum efficiency (EQE), which is defined as the ratio of electron-hole pairs generated to the number of incident photons hitting the front surface of the device, as a function of wavelength.[4] Figure 1 presents the AM 1.5 G solar spectrum and shows the spectral region where a standard perovskite solar cell (PSC) effectively absorbs light (E_g = 1.55 eV), as determined from its EQE spectrum, and the spectral

regions where DS and UC can be utilized to reduce spectral losses. The blue shaded region illustrates where DS can be used to convert high energy photons to photons closer to the bandgap energy, thus minimalizing thermalization losses. The red shaded region shows where UC is required to enable absorption of photons whose energy is lower than E_g.

Silicon cells, both crystalline (c-Si) and amorphous (a-Si) (E_g ~1.1 eV) exhibit high EQEs in the visible/near infrared (NIR) region (~450-1000 nm), with the efficiency decreasing gradually outside this window.[7] Thin film chalcogenide cells (*e.g.* copper indium gallium selenide (CIGS), copper zinc tin sulfide (CZTS)) (E_g ~1.55 eV) show an even narrower window of performance efficiency (~500-800 nm). [7] For organic photovoltaic devices (OPV), dye-sensitized solar cells (DSSCs) or inorganic-organic hybrid perovskite cells (PSCs), the spectral window can be tuned to some extent through careful selection of the light-harvesting dye. However, state-of-the-art PV cells exhibit a maximum EQE over a spectral window of ~400-750 nm for PSCs (E_g ~1.6 eV),[7] ~350-750 nm for OPV (E_g ~1.6 eV) [8] and ~450-800 nm for DSSCs (E_g ~1.55 eV).[9] As can been seen from Figure 1, at wavelengths higher and lower than the EQE spectrum, there is a rapid drop off in the fraction of the solar spectrum which can be harvested, and at all wavelengths lower than the bandgap, a significant portion of the solar spectrum is not absorbed. Although the specific spectral window varies for each class of PV cell, it is clear that all existing PV technologies suffer from reduced EQEs in the UV/blue and infrared portions of the solar spectrum. In addition to the thermalization losses described above, significant losses also occur at short wavelengths due to the encapsulation of the finished cell. These losses may include absorption from the glass or encapsulation material or increased reflectance or absorption from the anti-reflective coating.[4]

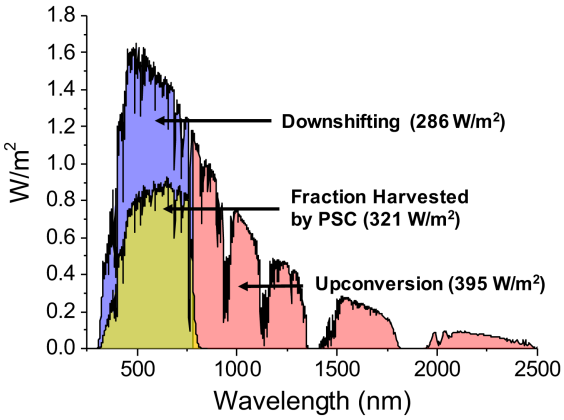

Figure 1. The AM 1.5G solar spectrum (solid black line), the fraction of incident radiation effectively harvested by a reference perovskite solar cell (yellow), and the spectral regions in which downshifting (blue) and upconversion (red) spectral converters can be exploited to improve the cell efficiency. The maximum fraction of the solar spectrum efficiently harvested by the PSC was determined from the product of the maximum fraction of incident photons which can be harvested by the cell (E_g = 1.55 eV) and the corresponding EQE spectrum.

All spectral converters exploit the process of photoluminescence to capture low- or high-energy photons that cannot be used effectively by the bare PV cell and convert them to photons of useful wavelength. Figure 2 presents a schematic illustration of the three photoluminescence processes currently under exploration for the development of efficient PV devices - down-shifting, quantum cutting and upconversion - and demonstrates the different architectures used to integrate the spectral conversion layer with a single-junction solar cell.

Down-shifting (DS) involves the conversion of one absorbed high-energy photon into one of lower energy that can be harvested more efficiently by the PV cell. Two different architectures have been widely explored to integrate down-shifting converters with PV cells: (1) a planar design, where the down-shifting material is applied as a luminescent coating on the top surface of the PV cell (usually called a luminescence down-shifting layer (LDS)[4] and (2) a luminescent solar concentrator (LSC) structure, in which the luminophore is either coated on, or doped within, a transparent waveguide slab, that has PV cell(s) coupled to its edges.[5]

Non-absorption losses in the low energy region of the spectrum can be remedied through the use of upconversion (UC) layers. The upconverting molecule absorbs two (or more) sub-

bandgap photons, converting them into one higher energy photon that can be absorbed by the PV cell. UC layers are usually placed beneath the PV cell to trap and transform any photons that are initially transmitted – a reflective layer ensures that the upconverted photons are directed back to the PV cell for use. Although a concentrator-type structure could also be suitable for UC materials, this architecture has received very little attention to date.[6] In addition, quantum cutting (QC) is a relatively recently identified process for spectral conversion,[10] in which thermalization losses can be reduced through the "cutting" of one single high energy absorbed photon into two (or more) lower energy photons (*i.e.* downconversion), which can be absorbed by the solar cell.

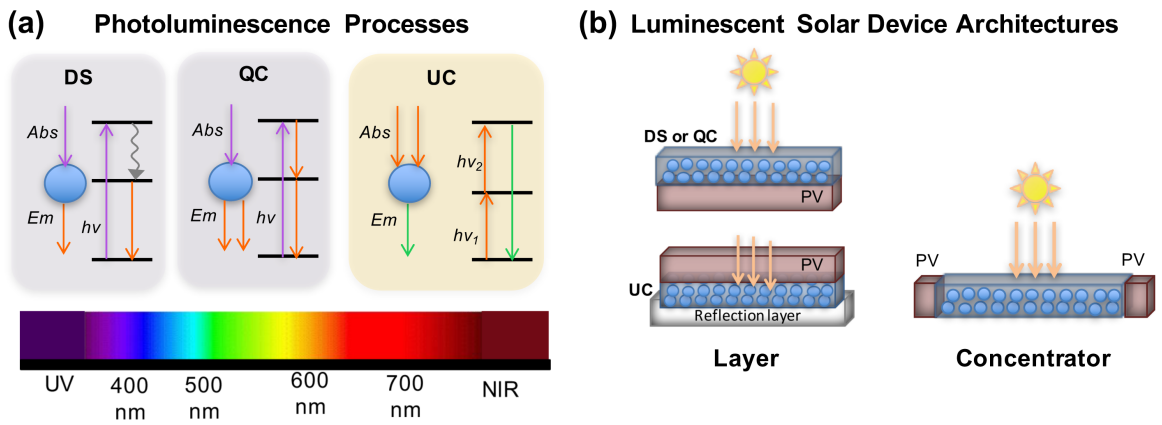

Figure 2. Photoluminescence processes employed in spectral converters and their integration with PV cells to form luminescent solar devices. (a) Simplified energy level diagrams for down-shifting (DS), quantum cutting (QC) and upconversion (UC). DS converters absorb a single high energy UV/blue photon and convert it to an emitted photon of lower energy. In QC, a single high energy photon is "cut" or downconverter into two (or more) lower energy photons. Conversely, UC materials absorb two (or more) low energy photons and convert them to one emitted high energy photon. (b) Layer and concentrator architectures are both used to couple spectral converters to PV cells. In the layer structure, DS or QC layers are coated onto the top surface of the solar cell, while UC layers are coated to the bottom/back side to capture any photons transmitted through the device. The reflection layer is included to ensure that any upconverted photons are directed back to the PV cell. The concentrator architecture is most commonly encountered for DS materials and comprises a transparent waveguide slab, doped or coated with the DS luminophore, and coupled to PV cells at one or more edge.

The potential enhancement in the PV cell conversion efficiency offered by each spectral conversion mechanism is not equal. While LDS layers can reduce energy losses due to surface, Auger or Shockley-Read-Hall recombination of electron-hole pairs,[11] the efficiency is capped by the photoluminescence quantum yield (PLQY) of the luminophore, which cannot exceed 100%. As such, the efficiency of luminescent solar devices (*i.e.* integrated spectral converter-PV cell systems) based on DS alone can never break the Shockley-Queisser barrier. In contrast, luminescent solar devices incorporating upconversion or quantum cutting materials, generate a higher number of photons (and therefore electron-hole pairs), which increases the short circuit current of the PV cell. Theoretical studies predict a maximum conversion limit of 47.6% and 39.63% for UC[12] and QC[13] materials, applied as layers on either the bottom or top surfaces of a c-Si cell, respectively, under non-concentrated irradiation.

In the following sections, we consider downshifting (in both LSC and LDS architectures) and upconversion approaches individually, first describing the fundamental physical and optical requirements of the materials used and then elaborating on new developments in materials design that have been used to advance each technology, particularly in terms of integration with PV cells. Since most studies on QC to date are restricted purely to materials characterization rather than integration with devices, we limit our discussion on this approach to its future perspectives.

3. Luminescent Solar Concentrators

3.1 Working principle and figures-of-merit

The basic structure of a conventional (downshifting) LSC comprises a transparent waveguide plate that is either doped or coated with luminescent molecules (Figure 3a). High energy photons incident on the plate are absorbed by the luminophores and subsequently remitted at longer wavelengths. A portion of the emitted light is guided *via* total internal reflection (TIR) to the edges of the waveguide, where a coupled PV cell(s) collect and convert the light to electricity. LSCs have the advantage of allowing sunlight to be harvested over large areas and

concentrated to small areas (geometrical concentration), thus reducing the area and number of PV cells required and making the use of high efficiency PV cells more cost-effective.[5] It should be noted that the efficiency of an LSC will always be lower than the equivalent area of an efficient PV cell. However, the flexibility in design and low cost could make them an important component of building-integrated photovoltaics in the future.

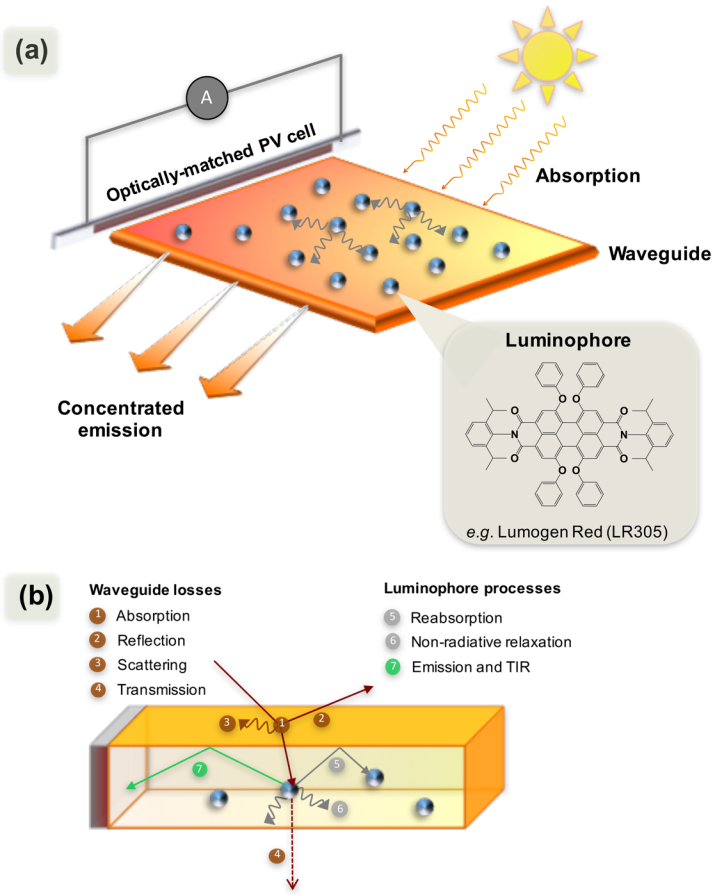

Figure 3. Operating principle of a luminescent solar concentrator (LSC). (a) Light incident on the LSC is absorbed by the luminophores and re-emitted at longer wavelengths. The emitted photons are propagated through the waveguide by total internal reflection (TIR), resulting in concentration of the emission at the slab edges. The concentrated emission can be used to sensitize an optically-matched PV cell, placed at one, some or all of the edges. (b) Primary processes and losses occurring in a planar LSC. Waveguide losses include absorption, reflection and scattering of the incident sunlight at the surface or internal defects, or complete transmission. Luminophore losses include low absorption or emission efficiencies (*e.g.* due to non-radiative relaxation), reabsorption of emitted photons by neighboring molecules or emission of photons within the escape cone of the waveguide.

Table 1 reports the figures of merit for a variety of state-of-the-art LSCs and shows the breadth of architectures and measurement conditions used in the literature to report performance. The performance of an LSC is quantified by the optical conversion efficiency (η_{opt}), given by:

$$\eta_{opt} = \frac{OP_{out}}{OP_{in}} \quad (1)$$

where OP_{out} is the total optical power output obtained over the sum of the four edges of the LSC and OP_{in} is the incident optical power falling on the top surface of the slab.[14,15] The influence of the dimensions of the LSC on the optical efficiency are accounted for by the geometric gain factor, G, which for planar and thin film LSCs, is given by:[14,15]

$$G = \frac{A_{surface}}{A_{edge}} \quad (2)$$

where $A_{surface}$ and A_{edge} are the area of the top surface and total area of the summed edges of the LSC, respectively. The overall performance of an LSC, taking into account the optical efficiency and the LSC geometry, can thus be quantified by the concentration factor, F:[14,15]

$$F = \eta_{opt} G \quad (3)$$

While η_{opt}, F and G are the figures-of-merit most commonly used to evaluate the performance of LSCs, at present there is no standardized protocol for experimentally-determining η_{opt}. Individual research groups use different experimental configurations in their testing including: full *versus* partial illumination of the device surface, single wavelength excitation *versus* full-spectrum illumination, full *versus* partial edge collection. Moreover, many groups do not report the G values for their devices and may use scattering backgrounds or reflective tape to boost the LSC performance.[16,17] While there are merits and disadvantages to each approach, the lack of consistency between reports makes it challenging to benchmark the performance of devices between laboratories. This is clearly a deficiency that needs to be addressed by the LSC community.

Table 1. Figures of merit for state-of-the-art LSCs in different architectures.

Architecture	Cell Type	λ_{ex} [nm]	η_{opt} [%]	*F*	*G*	PCE [%]	Comments	Reference
DCJTB, Pt(TPBP), Thin Film, Glass	c-Si	300-1400 (AM 1.5)	4.7	2.12[a]	45	6.8	Tandem LSC system	25
$M_6(II)X_{12}$ (M = Mo, W, X = Cl, Br, I), Thin Film, Glass	c-Si	300-1400 (AM 1.5)	-	-	25	0.44	Tested only with cell attached	29
CdSe/CdS QD, Doped, PMMA	-	300-1400 (AM 1.5)	10.2	0.13[a]	1.2[a]	-		30
PbS/CdS QD, Doped, Acrylate	-	300-1400 (AM 1.5)	6.1	0.61[a]	10	-		34
$CuInSe_xS_{2-x}$/ZnS QD, Doped, poly(lauryl methacrylate)	-	300-1400 (AM 1.5)	3.27	0.33[a]	10	-	Colorless LSC	37
TPE/PMMA, Thin Film, Glass	-	320	13.2	0.33[a]	2.5		AIE emitter	44
gem-pyrene ethene /PMMA, Thin Film, Glass	c-Si	300-1400 (AM 1.5)	-	-	25	0.32	AIE emitter	46
LR305/Urethane matrix (LT), Thin Film, Glass	mc-Si	300-1400 (AM 1.5)	2.48	0.67[a]	27[a]	0.49		69
F4Eu/F4Tb (F4 = silsesquioxane), Thin Film, Glass	-	290	1.2 /1.7	0.3 /0.43[a]	25a	-	Eu^{3+}/Tb^{3+} respectivel y	72
Eu^{3+} bridged silsesquioxane, Thin Film, Glass	-	300-380	12.3	3.08	25[a]	-		74
LR305, Doped, Di-ureasil	c-Si	300-800	14.5	0.48	3.3	0.54		19
EVA, LR305/PMMA, Thin Film, EVA	CIGS	300-1400 (AM 1.5)	-	-	-	8.14	CIGS cells aligned vertically	86
Ureasil, PMMA, Eu, hollow core cylinder	-	300-380	72.4	12.3	17[a]	-		14
Red LSC	DSSC	300-1400 (AM 1.5)	-	-	42	0.1		88

[a.] Calculated from reference. λ_{ex} is the excitation wavelength range. η_{opt} is the optical conversion efficiency, G is the geometric gain factor, F is the concentration factor and PCE is the power conversion efficiency.

3.2 The LSC materials toolbox –potential sources of loss?

The LSC toolbox is fairly simplistic – in principle with a suitable luminophore, waveguide and device architecture it is possible to optically concentrate sunlight. However, in practice, the optical conversion efficiency of any LSC is restricted by intrinsic loss mechanisms, illustrated in Figure 3b, many of which are related to the materials used. Luminophore-associated losses

include: incomplete harvesting of the solar spectrum, a low absorption efficiency and/or low photoluminescence quantum yield (Φ_{PL}), photodegradation of the lumophore, and reabsorption losses due to the absorption of emitted photons by neighbouring luminophores. The ideal luminophore should thus exhibit a broad absorption spectrum with a high molar absorption coefficient, a Φ_{PL} approaching unity, a large Stokes' shift (*i.e.* the separation between the band maxima of the absorption and emission spectra) to minimize reabsorption losses, and exhibit excellent photo- and thermal stability. The choice of luminophore will also determine the frequency of the emitted light and should thus be carefully selected to match the E_g of the coupled PV cell. to minimize thermalization losses. Waveguide losses include: escape cone losses leading to the non-capture of emitted photons, surface reflections and light scattering at internal and external defects and parasitic absorption. The ideal waveguide should thus have a high refractive index, be free of defects and exhibit a high transmittance across the full solar spectrum. As such, while the basic LSC design comprises just two components, the demands placed on the materials used are extremely high and there is considerable scope for innovation in this area. We note that there are several excellent reviews to which the reader is directed for a more comprehensive examination of the LSC field.[5,17,18] Here, we will focus on recent progress in the application of material design to the waveguide, luminophore and device architecture to address the intrinsic losses of LSCs.

3.3 New luminophore strategies

Since the conception of LSCs, π-conjugated organic dyes such as coumarins, naphthalimides, rhodamines and perylenes and perylene bisimides have been investigated extensively as potential luminophores.[5] Such molecules offer many attractive features for LSCs including high absorption coefficients, high Φ_{PL} and good photostability. The perylene bisimide, perylene-1,7,8,12-tetraphenoxy-3,4,9,10 tetracarboxylic acid-bis-(2'-6'diisopropylanilide), known commercially as Lumogen Red 305 (LR305, Figure 3a), is by far the most studied luminophore in LSCs due to its high photoluminescence quantum yield ($\Phi_{PL} \approx 97\%$ in

PMMA),[19] excellent photostability and red emission that is reasonably well-matched with the band gap of silicon photovoltaic cells (E_g ~ 1.1 eV).[2] However, LR305 exhibits an extremely small Stokes' shift, and as a result emitted photons can be reabsorbed by neighboring luminophores as they are transported *via* total internal reflection through the waveguide. While this does not necessarily translate into an intrinsic loss in itself, if the reabsorbed photons are not subsequently re-emitted, the Φ_{PL} is less than unity, or the emitted photons are directed within the escape cone of the waveguide, reabsorption will contribute significantly to the optical losses of the LSC. Moreover, organic luminophores such as LR305, show a strong tendency to aggregate *via* intermolecular π-π stacking interactions between the conjugated backbone of the molecule. Aggregation often leads to a reduction in Φ_{PL} due to the formation of non-emissive absorption centers, a phenomenon that becomes exacerbated at elevated luminophore concentrations or low solubility in the deposition medium.[20]

Given the key role of the luminophore in not only harvesting sunlight, but also concentration and transport, it is unsurprising that is has been the focus of the majority of recent research in this field. Aside from the vast array of organic luminophores already screened, there have been several pioneering approaches directed at overcoming the main limitations of archetypal organic dyes – namely small Stokes' shifts and associated reabsorption losses, aggregation-induced quenching of the photoluminescence and narrow absorption windows. We will now consider each of these approaches in more detail.

3.3.1 Stokes-shift engineering in inorganic luminophores

Reabsorption losses can be minimized by using luminophores with a small overlap between the absorption and emission spectra, *i.e.* those exhibiting a large Stokes' shift. This can be achieved through the strategic design of luminophores in which the absorption and emission processes occur from different energy states, localized either on the same or different chemical species. Trivalent lanthanide ions (Ln^{3+}) have been widely investigated as phosphors for LSCs due to their high photostability and large Stokes' shift.[18,21] However, the low molar absorption

coefficients associated with *f-f* transitions[22] prevent the practical application of isolated Ln^{3+} species in solar energy harvesting. This problem can be circumvented by exploiting the *antenna effect*,[22] in which coordinated organic ligands absorb light and transfer the energy to a Ln^{3+} center, from which emission occurs. This approach successfully harnesses the high molar absorption coefficients of the organic chromophore, thereby eliminating the low intrinsic absorbance of the Ln^{3+} ion. However, the energy transfer scheme requires the involvement of multiple energy states: photon absorption initially results in population of the first excited singlet state, S_1, on the ligand, which subsequently transfers its energy to the Ln^{3+} center, either directly from the S_1 state or *via* its first excited triplet state, T_1, following intersystem crossing (ISC).[21,23] Thus, while this energy transfer cascade results in a large Stokes' shift, careful matching of the participating energy levels is required to ensure that non-radiative relaxation processes do not detrimentally affect the Φ_{PL}. In reality, this is non-trivial, and photoluminescence quantum yields rarely approach unity for lanthanide complexes.[18,22] There are some exceptions: for example, Moudam *et al*. reported a highly red-emissive Eu^{3+} complex, Eu(hexafluoroacetylacetonate)$_3$(*bis*(2-disphenylphosphino)phenyl)ether oxide, which exhibited a Φ_{PL} = 86% when immobilized in a poly(methylmethacrylate) (PMMA) film, upon ligand excitation[24], while Correia *et al*. obtained a Φ_{PL} = 85% for Eu(tta)$_3$·2H_2O (tta = 2-theonyltrifluoroacetone) embedded in an organic-inorganic hybrid matrix.[14] An alternative approach is to use a room-temperature triplet-emitter, such as a transition metal complex or coordination compound.[23] The phosphorescent platinum tetraphenyltetrabenzoporphyrin (Pt(TPBP)) was successfully implemented as the emitter molecule in tandem LSCs by Currie and co-workers, resulting in power conversion efficiencies (PCEs) of 6.8%, 11.9% and 14.5% for c-Si, CdTe and CIGS cells, respectively.[25] Excitation of the singlet state of Pt(TPBP), coupled with the low absorption coefficient of the emissive triplet state produced a large effective Stokes' shift and minimized reabsorption in this LSC configuration.

Quantum dots (QDs) are also attractive candidates as luminophores for LSCs due to the possibility of engineering their photophysical properties through judicious choice of the material/architecture combination employed (*e.g.* by forming core/shell,[26] alloyed[27] or doped QD structures).[28] This structural versatility provides a way of tuning the E_g so that QDs that absorb and emit light across the entire spectral region may be designed.[15] Recent efforts on QD and nanocrystal LSCs have focused on the use of band-gap and Stokes-shift engineering to minimize optical losses resulting from reabsorption. Lunt *et al*. reported that hexanuclear metal halide nanoclusters of the form $M_6(II)X_{12}$ (M = Mo, W, X = Cl, Br, I) encapuslated in poly(butyl methacrylate-*co*-methacrylate)/poly(ethylmethacrylate) composites exhibited a massive Stokes' shift of ~400 nm, a Φ_{PL} > 75% and could sensitize a coupled Si cell to achieve a PCE of 0.44%.[29] "Giant" core-shell QDs, in which a large shell prepared from a wide bandgap semiconductor is grown on a relatively small core prepared from a narrower bandgap semiconductor (*e.g*. CdSe/CdS)[30–33] present another possible solution to the re-absorption dilemma. In these QDs, absorption occurs predominantly in the shell, while the red-shifted emission originates either from the core or from transitions occurring at the materials interface. Such heterostructures show zero- or negligible reabsorption, as the absorbing and the emitting states are decoupled from each other, leading to highly efficient LSCs. For example, Meinardi and coworkers prepared large-area LSCs (G = 1.23) from thick shell CdSe/CdS heterostructures (Φ_{PL} = 50%) immobilized within a PMMA host with a conversion efficiency per incident photon over 1%.[30] Monte Carlo simulations predicted a 100-fold increase in efficiency for the giant core-shell structures compared to the core-only analogues due to the minimized reabsorption losses. Zhou *et al*. designed a rectangular LSC based on NIR-emitting PbS/CdS core/shell QDs encapsulated in a poly(butyl methacrylate-*co*-methacrylate)/poly(ethylmethacrylate) (pLMA-*co*-EGDM) waveguide which exhibited Φ_{PL} of 40-50% and η_{opt} = 6.1 (G = 10) for the champion device, considering single edge emission and with the remaining three edges covered with reflective mirrors.[34] The size of the Stokes' shift

was shown to depend on both the core size and shell thickness. The addition of transition metal dopants in the form of substitutional defects can also be used isolate the absorbing center from the emissive state. For example, Erickson and coworkers showed that Mn^{2+}-doped ZnSe/ZnS core-shell QDs embedded within a pLMA-*co*-EGDM film (G = 22) exhibit zero reabsorption.[35] The ZnSe shell absorbs UV light (E_g ~3.1 eV) and efficiently sensitizes Mn^{2+} substitutional defects in its lattice, which emit at ~2.1 eV (~590 nm), resulting in a large effective Stokes' shift and Φ_{PL} of 50%. The same group showed that although the "giant" QD structure is effective at minimizing reabsorption losses at short transport lengths, at intermediate distances even the moderate core absorption can cause major reabsorption losses.[32] This could be mitigated to some extent through the addition of substitutional dopants to the core.

Although Stokes-shift engineered QDs appear to provide a solution to reabsorption losses, there are still several obstacles to be overcome. The first lies with the engineering challenge of physically incorporating the QDs within the processing medium, either the waveguide itself or the coating material. Core-shell heterostructures exhibit relatively moderate absorption bands and therefore significant dopant concentrations are required. However, at high concentrations, QDs tend to aggregate in the host matrix.[36] Branched organic co-polymers such as pLMA-*co*-EGDM inhibit aggregation to some extent, but there is a definite need to design new polymers which can improve this further. Moreover, interactions between the surface of the QD and the host medium can also result in a decrease in the Φ_{PL}. Meinardi and coworkers showed that this effect can be somewhat mitigated through surface passivation.[37] Colorless LSCs prepared from alloyed $CuInSe_xS_{2-x}$ QDs coated with a ZnS passivating layer incorporated in a poly(laurylmethacrylate) waveguide exhibited an optical power efficiency of 3.27% for G = 10 and maintained a Φ_{PL} of 40%. The final challenge facing conventional QDs is the toxicity of the metals used (*e.g.* Cd, Pb).[38] While an argument can be made that in LSCs the QDs are embedded in a host matrix and thus exposure to the wider environment is limited,

recyclability and correct disposal measures remain an issue. Researchers may look towards new classes of QDs based on carbon[39] or silicon,[40] which have a lower intrinsic toxicity.

3.3.2 Aggregation induced emitters – a single solution to reabsorption and aggregation losses?

Many organic luminophores form clustered aggregates due to intermolecular π–π stacking interactions between the aromatic rings of neighboring molecules. Aggregation may lead to either partial or complete emission quenching due to preferential relaxation *via* non-radiative channels.[20] However, for some organic molecules, aggregation can switch on emission from dormant luminophores leading to aggregation induced emission (AIE).[41] AIEgens (*i.e.* AIE active molecules) typically contain a highly twisted molecular core that hampers intermolecular π–π stacking interactions. Upon aggregation, the twisted core structure, combined with the synergistic effect of restricted intramolecular rotations and/or vibrations, reinstates emission from the molecule, which can be exploited in applications such as sensing and optoelectronics.[41–43] In 2014, Wong, Ghiggino and coworkers pioneered the use of AIEgens as luminophores in LSC devices.[44] In this initial report they showed that a thin film LSC prepared from the archetypal AIEgen, tetraphenylethene (TPE), cast in a PMMA film on a glass substrate (G = 2.5) was able to effectively concentrate light. However, as the emission range of TPE (~λ_{em} = 450 nm) was not well-matched for LSCs coupled with silicon or GaAs photovoltaic cells, they also investigated other contorted polyaromatic hydrocarbon dyes based on the TPE motif in an effort to extend the absorption window and shift the emission further to the red. While this was successful to some extent, with an increasing number of the polyaromatic rings (2–4), the solid-state Φ_{PL} was observed to decrease from 49.5 to 31.2%. The same group subsequently reported a twist on this method in which an AIEgen, 2-(4-(diphenylamino)phenyl)-3,3-diphenylacrylonitrile (DPATPAN), was used as an energy transfer donor for the highly emissive acceptor dye, 4-(dicyano-methylene)-2-tert-butyl-6-(1,1,7,7-tetramethyljulolidyl-9-enyl)-4H-pyran (DCJTB).[45] The donor-acceptor ratio was

optimized based on the measured quantum yield of the blend (max Φ_{PL} = 92%), with the concentration of the non-AIE acceptor dye kept low to minimize aggregation and reabsorption losses. Distance-dependent EQE measurements on finished LSC devices showed that the high absorbance of the DPATPAN donor greatly reduced transmission losses leading to a substantially improved light-harvesting performance. More recently, the group have reported a transparent planar concentrator using H-aggregates of *gem*-pyrene ethenes, which display excimer-like emission with Stokes' shifts greater than 1 eV.[46] Planar LSCs were prepared by casting a thin film of the *gem*-pyrene ethane in PMMA (50 % w/w)) onto a glass substrate (Φ_{PL} = 52%), which was subsequently adhered to silicon PV cells, electrically-coupled in parallel. A power conversion efficiency (PCE), of 0.32% was obtained, where the PCE is the ratio of generated electrical power to incident light power.

While there are just a few examples of AIE-based LSCs to date, this approach not only offers significant potential for overcoming aggregation-induced concentration quenching, but will enable the use of higher luminophore loadings, thereby increasing the light-harvesting efficiency. Moreover, when used in conjunction with energy transfer, a large effective Stokes' shift may be induced, thereby eliminating optical losses due to reabsorption. Clearly, there are still challenges to be overcome, particularly in the identification of red-emitting AIE-gens with high Φ_{PL}. However, as the library of AIE-gens is expanding rapidly,[41–43] providing more insight into the design rules dictating this phenomenon, it seems unlikely that molecules exhibiting the requisite optical properties for LSCs will remain elusive for much longer. Moreover, a large variety of AIEgens possessing optical waveguide effects, with emission colors spanning the whole visible spectrum have also been developed.[47–50] Thus AIE-gens may offer the unique potential of combined emission and waveguide properties from a single material for LSC applications.

3.3.3 Tuning the effective Stokes' shift using energy transfer cascades

We have already seen some examples of LSCs where a blended "cocktail" of molecular luminophores can be invoked to overcome the problem of reabsorption through intermolecular Förster energy transfer (FRET).[25,45] However, the high luminophore concentrations required to bring the donor and acceptor molecules within spatial proximity required for FRET may not always be feasible in terms of solubility and cost. An alternative approach is to use a multichromophoric system in which efficient excitation energy transfer (EET) cascades occur from energy donors to covalently-linked acceptors. In this approach, chromophores exhibiting different HOMO-LUMO gaps are employed to create an energy gradient through which excitation energy can be shuttled. Such systems are designed to mimic the role of the light-harvesting chromophoric scaffolds found in plants and photoactive bacteria.[51] There have been several reports of dendritic structures that exhibit a Stokes' shift that is large enough to reduce reabsorption.[52–56] For example, Akkaya *et al.* reported a dendritic system composed of boron-dipyrromethene (bodipy) dyes with varying degrees of functionalization with styryl groups. Each bodipy dye absorbs in a different part of the visible spectrum, ensuring a broad absorption window; however efficient EET through the individual units leads to emission only from the terminal absorber.[53] However, such dendritic systems are challenging to synthesize and the Φ_{PL} is typically low (max Φ_{PL} = 32%), limiting their practical application in LSCs. Nonetheless, smaller molecular analogues may present a viable alternative. Shenning and coworkers recently reported a switchable LSC based on a multichromophoric triad comprised of two perylene bisimide donors and one orthogonal perylene bisimide acceptor, incorporated in a commercial nematic liquid crystalline host.[57] The absorbing donor state could be switched from "off" to "on" by applying a voltage across the liquid crystal cell, which caused the molecules to reorient in a homeotropic orientation, perpendicular to the cell surface. Upon triggering the donor absorption, the energy transfer efficiency to the acceptor was close to unity. Notably, the devices maintained contrast in transmission between "on" and "off" states. The energy transfer cascade approach has also been used to develop LSCs from thin film blends of luminescent

conjugated polymers and molecular dyes.[58] Two poly(arylene ethynylene)s of different optical bandgap were chosen as the primary light-harvesting component, through which excited electrons were rapidly shuttled along the delocalised π-electron backbone to a lower energy state, which subsequently underwent energy transfer to the dye LR305. The luminophore cocktail, combined with the molecular wire effect associated with the conjugated polymer resulted in a broad absorption window and sufficient Stokes' shift to minimize the effects of reabsorption.

However, while energy transfer in multichromophoric systems or "molecular cocktails" can lead to large effective Stokes' shifts, the synthetic demands and the lack of controlled luminophore placement, respectively, may limit the practical viability. Controlled supramolecular assembly of individual donor and acceptor components through weak physical interactions, as demonstrated recently for amino-acid functionalized chromophores (*e.g.* perylene bisimide[59,60], coumarin[61]), may provide an effective compromise to the two extremes.

3.4 Advances in waveguide design

The key requirements for the waveguide are a high light-trapping efficiency and optical transparency across a broad spectral range. In addition, as the waveguide acts as a host or support material for the luminophore, processability and stability are also important. The light-trapping efficiency, given by $\eta_{trap} = (1-1/n_\lambda^2)^{1/2}$, where n_λ is the refractive index at wavelength, λ, is a measure of the fraction of emitted photons confined within the waveguide by TIR. Photons emitted by a luminophore within the escape cone will be lost through the front and back surfaces of the LSC. Escape-cone losses occur for light rays intersecting the waveguide surface at angles $\theta_i \leq \theta_c$, where θ_c is the critical angle given by $\theta_c = \sin^{-1}(1/n_\lambda)$. Reflection of incident photons at the waveguide surface represents another loss and is described by the Fresnel reflection coefficient (R) for perpendicular incidence, given by $R = (1-n_i)^2/(1+n_i)^2$, where n_i represents the refractive index of the medium at the incident wavelength. Based on

these relationships, the refractive index of the waveguide medium is clearly paramount, and the optimum range for LSC applications is n = 1.5-2.0. This range allows for the maximum trapping efficiency with minimized reflective losses at the top surface of the LSC.

The waveguide choice has received significantly less attention than the luminophore and cheap polymers such as PMMA, and to a lesser extent poly(carbonate) (PC), are most commonly used.[5] There is therefore a huge opportunity to overcome waveguide losses, or to deliver improved stability, through the implementation of unexplored materials whose optical and physicochemical properties are specifically tailored for LSC applications. In this category, we will consider both new polymers and organic-inorganic hybrid materials as waveguides. We will also discuss how the waveguide offers the possibility for directing the placement of the luminophore, through patterning, the application of electrical fields or chemical modification.

3.4.1 Polymer waveguides

PMMA and PC have refractive indices on the lower boundary of the useful range for LSCs (n = 1.49 and 1.59, respectively).[62] An obvious, but underexplored, approach to decrease waveguide losses is to substitute these with a high refractive index polymer, such as a sulfur-containing polyimide or poly(arylene sulfide).[63] The environmental impact of any new technology should also be considered and biodegradable polymer waveguides may potentially reduce the carbon footprint of LSCs. Camaioni *et al*. investigated the suitability of L-poly(lactic acid) (L-PLA), a carbohydrate derived from starch, as a transparent waveguide matrix for LSCs.[64] L-PLA-based films, both chemically modified or blended with a photoluminescent oligothiophene showed excellent processability, photostability, and reasonable photoluminescence quantum yields (Φ_{PL} = 35%). However, L-PLA has only a moderate refractive index (n = 1.45) and is processed from organic solvents. To overcome these limitations, the same group demonstrated that silk fibroin from the *Bombyx mori* silkworm could also be functionalized with an oligothiophene dye to generate an LSC.[65] The silk fibroin

films showed high optical transparency in the visible range, a high refractive index (n = 1.54 at 633 nm and water-processability.[66]

Degradation of the luminophore and the polymer waveguide under continuous illumination severely affects the device stability. Although PMMA is considered the gold standard waveguide material for LSCs, it is susceptible to photo- and thermal oxidation[67] after prolonged light exposure, which give rise to the formation of photon trap sites which reduce the transport efficiency.[68] As such, alternative, high stability waveguide materials that can deliver long term performance must be developed. Griffini *et al*. reported the use of cross-linked fluoropolymer-based matrices as host materials for thin film LSC devices.[69] After optimizing the luminophore concentration and film thickness, efficiency values comparable to a reference PMMA-based LSC were achieved, along with superior under long-term stability under continuous illumination (500 h).

3.4.2 Organic-inorganic hybrid materials

The stability question raised by organic polymer waveguides has led to the investigation of inorganic glasses (*e.g.* silica-zirconia and silica-titania)[70] and organic-inorganic hybrids[18] as potential alternatives as waveguides. While pure glass waveguides have a high refractive index, their weight and fragility limits their useful application in building integrated photovoltaics.[5] In contrast, organic-inorganic hybrids offer the best of both worlds, combining processability and chemical functionality from the organic component, with optical transparency and high stability from the inorganic one.[71] Carlos and coworkers first introduced the use of luminescent bridged-silsesquioxane thin films doped with trivalent lanthanide ions as LSC materials.[72,73] Single wavelength excitation (290 nm) η_{opt} values of 1.2% and 1.7% were obtained for Eu^{3+}- and Tb^{3+}containing films, respectively.[72] More recently, the same groups reported a superior silsesquioxane system based on an ethane tetracarboxamide-based organosilane doped with Eu^{3+} ions.[74] Thin films (~200−400 nm) spin-coated on glass substrates led to highly luminescent coatings with Φ_{PL} = 0.60 and an optical conversion efficiency of 12.3% (excitation:

300−380 nm). Organic-inorganic hybrid waveguides from the ureasil family have also been doped or coated with organic dyes [19] and Eu^{3+} β-diketonate complexes[75,76] to produce LSCs. Ureasils are comprised of a siliceous skeleton that is chemically-grafted to poly(ethylene oxide) (PEO)/poly(propylene oxide) (PPO) chains through urea cross-linkages. A planar, doped LSC based on LR305 doped in a di-ureasil (two urea bridges) waveguide exhibited an η_{opt} = 14.5% (emission: 300–800 nm, G = 3.3) for the optimized device (Figure 4).[19] A power conversion efficiency (PCE) of 0.54% was obtained for the champion LSC coupled to a c-Si PV cell using the di-ureasil precursor as an optical glue to minimize interfacial losses. Despite the limited use of hybrid materials in LSCs to date, their efficiency values are already comparable to those of pure organic LSCs.[19,72] The huge variety of organic precursors available both commercially and through custom synthesis introduces the possibility of tuning the functional and mechanical properties (*e.g.* strength, flexibility, porosity) of the hybrid. Moreover, the use of mixed metal oxide sol-gel precursors (e.g. silica-titania, silica-zirconia) provides a means of tuning the refractive index.[70] Organic-inorganic waveguides thus offer the potential to deliver tailored properties for LSCs in a single material.

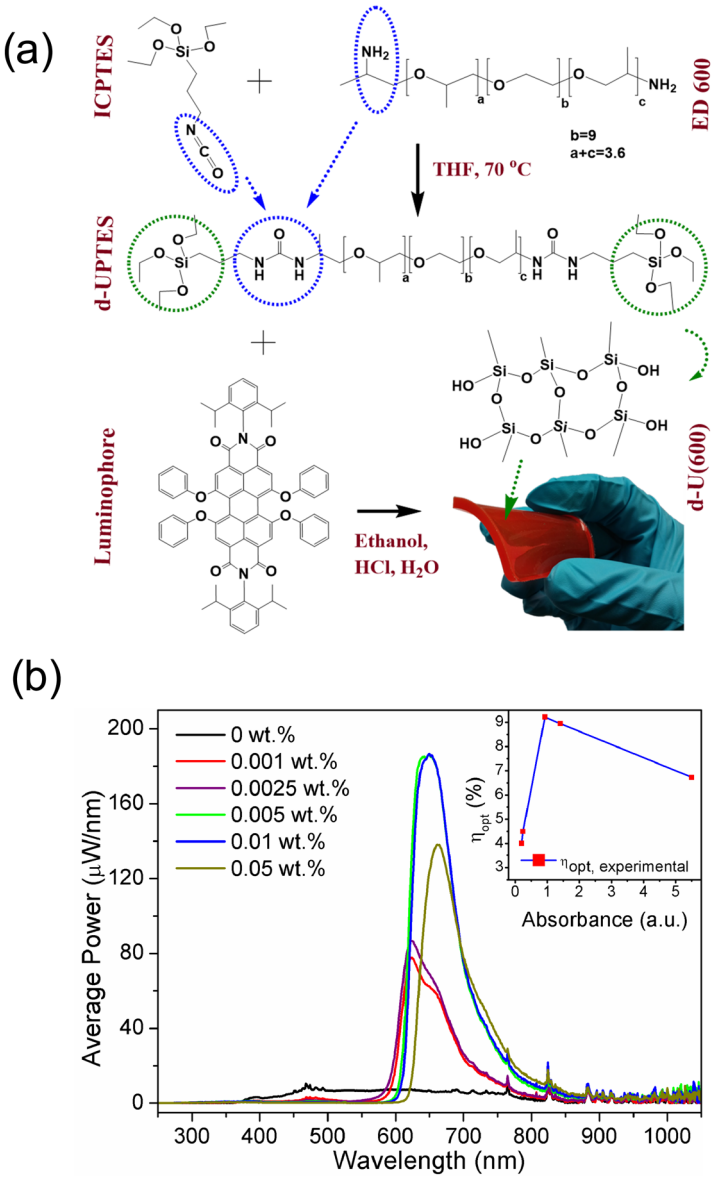

Figure 4. Synthesis and characterization of LR305-di-ureasil planar waveguides. (a) Schematic representation of the LSC fabrication. In the first step, the precursors Jeffamine ED-600 and ICPTES are reacted to obtain di-ureapropyltriethoxysilane (d-UPTES). Following the dissolution of the luminophore, LR305, in d-UPTES, acid-catalyzed hydrolysis and condensation of the siliceous network is initiated to obtain the LR305-d-U(600) LSC. (b) Optical power spectra of doped LR305-d-U(600) LSCs with a dark absorbing background, averaged over all four edges. (Inset) Variation of the experimental optical (red squares) efficiencies of the LSCs with a dark background, determined over the 300–800 nm spectral range, with respect to the LSC absorbance. Adapted with permission from reference 19.

3.4.3 Controlled luminophore placement within the waveguide

Reabsorption and FRET processes require alignment of the absorption and emission transition dipole moments of the luminophore.[77] Since, the transition dipole moment is often directionally aligned along the molecular backbone of organic molecules, controlled alignment or placement of luminophores within a host material may be used to inhibit or enhance these processes as required. Luminophore alignment may also help to reduce surface losses by ensuring emitted photons are not released within the escape cone. The most simple approach is to physically place thin film luminophore layers into spatially separated patterns on the waveguide surface.[78] However, while reabsorption losses decrease with a reduction in surface coverage, this also leads to a decrease in the total absorption and thus efficiency of the device. Organic host-guest systems have also been reported, in which the physical isolation of blue-, green- and red-luminophores within the layered host, deoxycholic acid (DCA), resulted in efficient FRET cascades.[79] DCA forms bilayer structures in the solid state with alternating stacks of hydrophobic and hydrophilic layers, within which molecular cavities are formed. Judicious selection of luminophores with the correct dimensions and polarity allows their controlled placement within either hydrophobic or hydrophilic cavities, facilitating optimization of the FRET process. Covalent grafting has also been investigated as a means of controlling the placement of luminophores within the organic-inorganic ureasil waveguides.[80] A perylene carboxdiimide-bridged triethoxysilane (PDI-Sil) was grafted to the siliceous domains of the ureasil backbone (Φ_{PL} = 76-87%). Through strategic variation of the branching and molecular weight of the organic poly(oxyalkylene) backbone, it was shown that the efficiency of energy transfer from the ureasil host to PDI-Sil could be modulated, tuning the emission color from pink to orange.

The use of liquid crystalline (LC) host materials to control the orientation of luminophores has also been investigated for light management in LSCs.[81–84] Planar luminophores typically orient parallel to the alignment direction of the LC, such that their primary absorption and emission transition dipole moments are also parallel aligned. This

configuration can lead to improved light concentration at the corresponding waveguide edges.[81,85] Alternatively, luminophores can be aligned perpendicular to the waveguide surface, which can reduce surface losses to <10%;[85] however this configuration leads to low light absorption and correspondingly low efficiencies due to misalignment of the absorption dipole moment with the incident light. This problem can be offset to some extent through the use of a two dye system, in which the absorption axes of each dye are aligned parallel and perpendicular to the host LC matrix, respectively.[83] Electrically-switchable systems were prepared by immobilizing LR305 (perpendicular alignment) and a coumarin derivative (parallel alignment) in a photopolymerizable LC host. While only a small change in the absorbance of LR305 is observed, the coumarin dye shows a more significant anisotropy in its absorption states depending on the alignment induced by the applied voltage. More recently, circular arrangements (prepared by the rub-alignment method) of a coumarin dye embedded in a photopolymerisable LC host coated on a waveguide were shown to effectively concentrate the emitted light to the waveguide center (Figure 5).[84] A cone shape-void was drilled into the center of the waveguide to enhance out-coupling of light and a solar cell was placed on its surface for photosensitization. Selective irradiation of the aligned LSC resulted a constant open circuit voltage (V_{OC}), but increased the short-circuit current (I_{SC}) by ~33% for silicon and III-V PV cells.

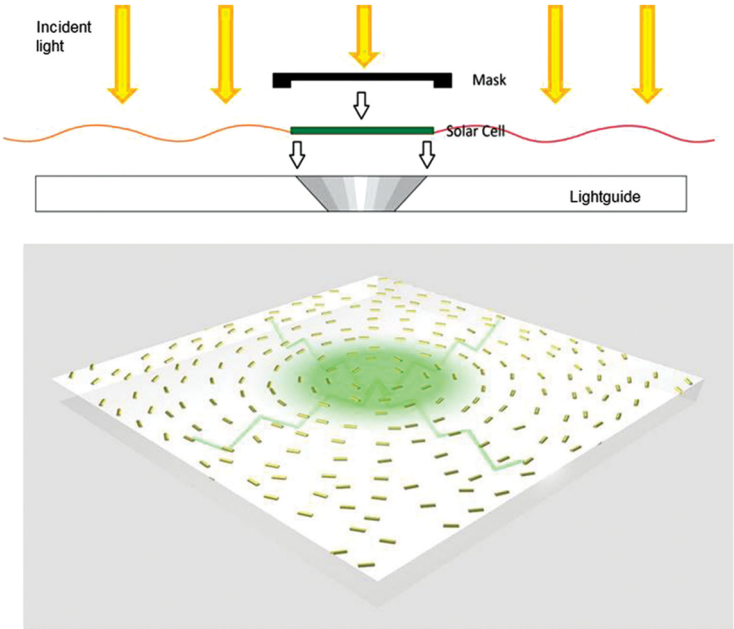

Figure 5. Schematic representation of a circularly aligned "theater" LSC. Fluorescent molecules are shown by yellow cylinders, the green lines are their emission and the green tinted region shows the area of enhanced light concentration. A PV cell is placed above a cone-shaped hole drilled in the LSC center to capture the concentrated light. Adapted with permission from reference 84.

3.5 New device architectures: towards integration with emerging PV technologies

The most commonly studied architecture is a planar luminescent waveguide, with the PV cells attached at the plate edges (Figure 3a). Recently, alternative architectures have been investigated, with the aim of improving performance, increasing functionality or facilitating integration with third generation photovoltaics. From a fabrication point of view, it would be more convenient for the coupled PV cells to be in-plane with the LSC, *i.e.* the active surface orientated in the same direction as the top surface of the LSC. This requires, however, a small modification in the device architecture to ensure that the emitted photons are captured by the cell. Jimenez-Solano and co-workers achieved this by developing a PV module that combined an LSC (LR 305 in PMMA, 2 μm thick) sandwiched between ethylene vinyl alcohol-coated glass covers, with two CIGS cells placed in-plane with the LSC, separated by an air gap.[86] The performance of the LSC was enhanced by coupling the luminescent film to nanostructured photonic crystals made of a periodic structure of alternating porous titania and silica

nanoparticle layers, that simultaneously enhanced light absorption at shorter wavelengths and light-guiding at longer ones. Optimized modules showed incident to guided photon efficiencies around 28% higher than those containing no photonic crystal layer (PCE = 8.14%). Yoon and coworkers reported a composite luminescent concentrator PV system, in which interconnected arrays of microscale silicon PV cells were embedded in a thin film of polyurethane doped with the organic dye, 4-dicyanomethylene-2-6-p-diaminostyryl-4H-pyran (DCM).[87] The PV cells were embedded close to the surface of the layer, such that their direct excitation by incident sunlight was also possible. The collection efficiency of the composite device, when coupled to a backside reflector, was ~17%, significantly higher than the efficiency of the analogous device containing no DCM (~3.5%).

Cylindrical LSCs display higher concentration factors than planar LSCs with the equivalent collection area and volume.[75] Correia *et al*. reported the fabrication of large area LSCs (length up to 2.5 m) in which bulk and hollow-core, cylindrical optical fibers were coated or filled with an active layer comprised of either Rhodamine 6G or $Eu(tta)_3 \cdot 2H_2O$ doped in a ureasil hybrid matrix (Figure 6).[14] For the bulk-coated LSC, light propagation along the entire fiber length was observed, with a maximum η_{opt} of 0.6% (F = 6.5). In contrast, for hollow-core LSCs light propagation was restricted to shorter distances ($6\text{-}9 \times 10^{-2}$ m) due to attenuation by the ureasil matrix. Optimized hollow-core devices displayed a maximum η_{opt} of 72.4% (F = 12.3), demonstrating the considerable potential afforded by fiber optic LSCs for commercial scale-up. Optical fibers also provide a suitable means of integrating LSCs with emerging PV technologies such as DSSCs, which cannot easily be fabricated as thin, robust strips. Peng and coworkers reported the combination of fiber DSSCs with commercially-available LSCs using a connective envelope or "groove" made from aluminium foil.[88] A maximum power of 10 mW (PCE = 0.1%) was reported for a red solar module (70.56 cm^2) coupled with four optical fiber DSSCs on each edge (5.50 cm).

Complementary light management techniques, such as surface plasmon resonance (SPR) and Bragg reflectors can also be integrated with LSCs to enhance their performance. Chen *et al*. recently reported the fabrication of electrospun organic nanofibers comprised of poly[2,7-(9,9-dihexylfluorene)-alt-4,7-(2,1,3-benzothiadiazole)] nanoparticles as the LSC and Ag nanoparticles for the SPR effect.[89] The nanofibers were integrated into OPV cells as an aligned, check-patterned network, leading to a power conversion efficiency (PCE) of up to 7.12%, an 18% enhancement compared to the parent device. Photonic nanostructures such as 3D opals have also been integrated into LSCs to modify the angular emission profile of the luminophore, such that the emitted photons are coupled more effectively into the TIR of the waveguide.[90] Photonic nanospheres have been used to extend the spectral range of collection of LSCs. Bozzola and coworkers coated an LSC with a monolayer of self-assembled polystyrene nanospheres, whose role was to promote forward diffraction into the waveguide slab at wavelengths not absorbed by the luminophore.[91] The wavelengths of the diffracted light were tuned by changing the diameter of the nanospheres, with an optimum diameter of 700-800 nm found to effectively diffract NIR photons into the waveguide.

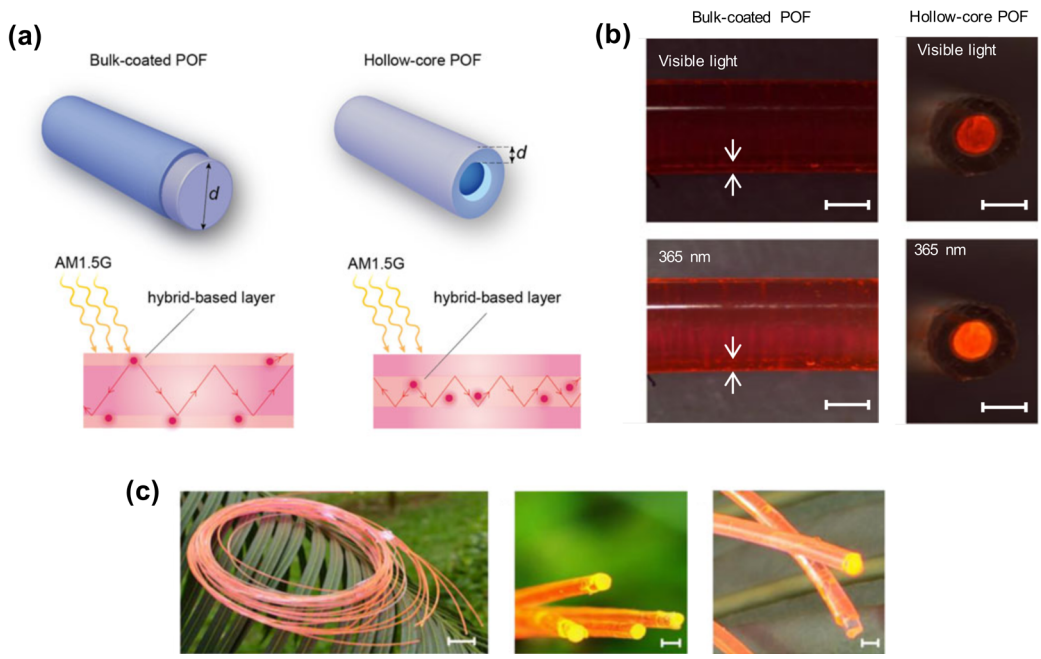

Figure 6. Bulk-coated and hollow-core PMMA-based optical fibers (POF). (a) Schematic representation of POF structure. The LSC layer is a Rhodamine 6G (red circle) doped ureasil hybrid coated at the surface of the POFs or

embedded into its hollow core. (b) Photographs of bulk-coated and hollow-core POFs under illumination with white light and at 365 nm. The arrows indicate the active layer; scale bars of 5×10^{-4} m. (c) Outdoor photographs of bulk-coated POFs. Scale bars of 10^{-3} m. Adapted with permission from reference 14.

4. Luminescent down-shifting

4.1 Working principle and figures-of-merit

In its simplest architecture, LDS is achieved by coating a photoluminescent layer on the top surface of a PV device (Figure 2). As such, LDS layers do not rely on the same geometric concentration as LSCs to improve cell efficiency, but are instead used to tune the window of spectral absorption, particularly in the UV/blue spectral region where most PV cells show low EQE.[1] Lower energy photons emitted by the luminophores after absorption are subsequently absorbed by the PV cell, producing more electron-hole pairs and thus generating an increased I_{sc}.[4] This should lead to an improvement in the EQE of the device in the absorption window of the LDS layer, although experimentally this is not always observed.[92] The V_{oc} and fill factor (*FF*) should not change significantly upon incorporation of an LDS layer since these depend primarily on the intrinsic materials of the PV cell itself.[4]

The LDS efficiency is quantified by relative changes in the EQE and IV curves measured before and after coating.[92–94] This allows for more consistency between the characterization protocols used for LDS than LSCs. The EQE, in particular, measures the λ-dependent response of a PV cell and thus enables the role of the LDS layer to be quantified directly. The requirements for an effective LDS luminophore are similar to those for LSCs: (i) strong absorption in the region(s) of interest for the PV cell; (ii) large Stokes' shift to minimize reabsorption loses, (iii) a high Φ_{PL}; (iv) high optical transmittance of the host material; (v) high photostability.[3,4] LDS luminophores fall into the same categories as those used for LSCs, with the most common being organic dyes[94–96], quantum dots [97–100] and lanthanide metal ions/complexes.[101–104] The host materials used for LDS have no need for long range TIR as

geometric concentration is not involved; however, a suitable refractive index (n =1.4-2.4) is still required to minimize both surface reflection and escape cone losses.[105] Typical host materials include polymers,[106–109] silica hybrids[110–112] or glasses,[103,104,113] although there are also numerous examples of luminophores coated directly onto the device surface.[93,114] If a host material is used, its thickness must be optimized to minimize edge emission.[4,115]

Recent research has focused on the optimization of host-luminophore combinations, with the aims of improving the stability, efficiency and ease of device fabrication. LDS layers must be tailored to the cell type used, and as such, there is no one size fits all approach. Table 2 summarizes the figures of merit for a variety of LDS systems with different PV devices. In the following sections, recent materials' advances in LDS technology will be described, categorized according to the PV cell that the luminophore-host combination is tailored towards.

Table 2. Figures of merit for state-of-the-art LDS coatings with different cell types, indicating the absolute power conversion efficiency (PCE) achieved and the percentage increase in PCE (ΔPCE) compared to the bare device.

Cell Type	Luminophore	λ_{abs} (nm)	λ_{em} (nm)	PCE (%)	ΔPCE (%)	Reference
c-Si	$Gd_2O_2:Eu^{3+}$	350	625, 700	12.79	23	101
c-Si	Si QD	400-1000	850	3.8	23	122
CIGS	Lumogen Violet / Lumogen Yellow	350-475	475-600	-	2.93	94
GaAs	CdSe/ZnS QD	350	540	18.05	25	114
InGaP	CdS_xS_{e1-x}/ZnS QD	350	580	15.6	15	123
DSSC	CdSe/ZnS QD	350	500	2.98	5	129
DSSC	Lumogen Violet	370	430	4.5	68	106
DSSC	EuD_4TEA	350	620	3.41	62	128
OPV	$C545T:Alq_3$	300-500	575	3.82	15	136
OPV	C QD	350	550	3.18	12	135
PSC	YVO_4/Eu^{3+}	295	610	7.93	7	140
PSC	$ZnGa_2O_4:Eu^{3+}$	400	610	13.8	29	141
PSC	Lumogen Violet	370	450	18.7	8	142

4.2 Silicon Photovoltaic Cells

As Si-based photovoltaics currently make up 90% of the global market,[116] significant research has been dedicated to the design of LDS systems for these cells. Theoretical calculations to determine the maximum efficiency gains possible by applying LDS layers to Si PV cells predict an increase of 0.6-1%.[117] Initial studies used isolated Eu^{3+} or Eu^{2+} ions doped in polymer hosts as the LDS layer; however the low absorption coefficients associated with free lanthanide ions limited the efficiency.[118,119] The use of Eu^{3+} or Eu^{2+} phosphors or complexes, however, has delivered improved performance. Chen *et al*. reported a Ba_2SiO_4:Eu^{2+} LDS layer coated directly onto a Si PV cell, in which the addition of Ag nanoparticles and a SiO_2 spacer increased the PCE of the cell from 17.1% to 17.7%.[120] An LDS layer comprised of Gd_2O_2S:Eu^{3+} with a Φ_{PL} = 26.6-32.6%, doped in poly(vinylpyrrolidone) and spin-coated onto a polycrystalline Si cell (PCE = 10.44%) was also reported.[101] The Gd_2O_2S:Eu^{3+} phosphors formed spherical particles and improved both the antireflection properties and I_{sc} of the cell, increasing the PCE to 12.97%. While most studies have focused on Eu^{3+} or Eu^{2+} as the luminophore, other lanthanide ions have also been investigated and perform comparably. For example, recently Fix *et al.* showed that LDS layers prepared from $[LnL_3](Et_3NH)_3$ (Ln = Eu, Tb) (L = triazole-pyridine-bis-tetrazolate antenna) doped in ethylene vinyl acetate (EVA) by spin-coating delivered a moderate increase in the PCE from 9% to 9.51% and 9.42% for Eu^{3+} and Tb^{3+} analogues, respectively.[102]

Recent attention has shifted to the use of QDs as luminophores for LDS layers. Detailed studies of CdTe or CdSe/CdS QDs doped in PMMA or EVA for both Si PV and CdTe/CdS thin film solar cells have been performed and suitable figures of merit to characterize the performance of LDS layers were proposed.[121] However, as described earlier, the solubility of QDs into polymer matrices can often be limited.[25,45,92] Draaisma *et al.* addressed the aggregation of QDs in host materials by exchanging capping ligands on $CuInS_2$/ZnS QDs with thiol-functionalized oligocaprolactone to increase solubility within a UV-curable acrylate resin host.[92] Unfortunately, the resultant LDS layers showed an overall decrease in PCE when

applied to the cell. However, this study demonstrates that careful control of the absorption properties, in particular the $\Phi_{PL,}$ of the QDs and adhesion of the layer to the PV cell are crucial to obtain improved efficiencies.

The synthesis of QDs is often challenging and can require inert atmospheric conditions.[99,112] Thus, significant attention has focused on the development of facile synthesis routes to QDs for LDS. The Li group recently synthesized red-emitting CdSe/CdS/ZnS QDs though microwave synthesis, which led to highly reproducible products. Although the QDs displayed only a moderate Φ_{PL} of 25.4%, when doped into a silica matrix and coated on a Si PV cell, an increase in the PCE of 0.8% from 15.34% to 16.14% was observed.[112] The same group reported an air-exposed, one-pot, microwave synthesis of $CuInS_2$/ZnS QDs, which showed high absorption at λ <400 nm, high Φ_{PL} of 56% and emission in the red/NIR region.[99] Upon incorporation into a PMMA host and coating on a Si PV cell (PCE = 15.6%), a PCE increase to 16.21% was observed. These QDs had the additional advantage of low toxicity compared with Cd-based alternatives. Although the above fabrication methods are facile and reproducible, they are not easily up-scaled, which presents a barrier to the large-scale development of QD-based LDS layers. To address this, Levchuk *et al.* demonstrated an easily scalable one-pot synthetic route to fabricate Mn^{2+} doped $Zn_xCd_{1-x}S$/ZnS nanocrystals.[93] The QDs showed Φ_{PL} of up to 70% and the synthesis gave consistent results when scaled up to 40 times the initial volumes. The QDs were applied directly to Si PV cells using the doctor blading method and an increase from 13.8% to 14.3% in the PCE was observed.

LDS layers are often applied to cells in conjunction with other surface modifications to minimize reflectance and maximize luminophore absorption. Xu *et al*. patterned the Si substrate by nanosphere lithography to lower surface reflectance and applied a Si-QD/SiO_2 composite layer.[122] A PCE increase from 3.1% to 3.8% was observed, demonstrating that LDS can be used effectively in conjunction with other light management techniques to improve the overall efficiency.

4.3 Thin Film Solar Cells

Thin film chalcogenide solar cells are potentially more suited for LDS applications as they typically exhibit narrower EQE ranges than Si cells.[4] Although attention has shifted from organic luminophores for Si PV cells, they continue to be investigated for thin film cells to improve the low wavelength response, particularly in blends which maximize the absorption efficiency and achieve near-unity Φ_{PL}. Lumogen® dyes, in particular, are often used to test new architectures as their properties are well-known and they are compatible with most polymer hosts. Parel *et al*. combined LSC and LDS properties in a so-called concentrating LDS layer (C-LDS).[96] The C-LDS layer consisted of Lumogen® dyes (Violet 570, Yellow 083 and Orange 240) doped in a PMMA plate placed on a CdTe cell. The geometric concentration occurs by placing a large area LDS plate on a smaller area solar cell in a planar architecture. Up to a 20% increase in the I_{sc} of the cell was obtained, demonstrating the potential of this architecture.[96] Thick LDS films of prepared from combinations of Lumogen® dyes (Violet 570 and Yellow 083) in polyvinyl butyral (PVB) were also applied to CIGS cells.[94] A Φ_{PL} of 96% was obtained and a 2.93% relative increase in PCE was observed, which was in good agreement with simulated predictions. Organic luminophores are also used to benchmark most theoretical modelling approaches developed for LDS. Richards and co-workers compared experimental results of six organic dyes, alone and in mixtures ($\Phi_{PL} \geq 87\%$), in two polymer hosts, and with three different cell types, with theoretical models based on ray-tracing simulations and two novel methods based on an analytical description of the LDS layer and a collection of figures-of-merit that address one or more of its desired properties (Figure 7).[95] The models were shown to predict the obtained I_{sc} to within 5%, thus, establishing a systematic approach to studying LDS systems.

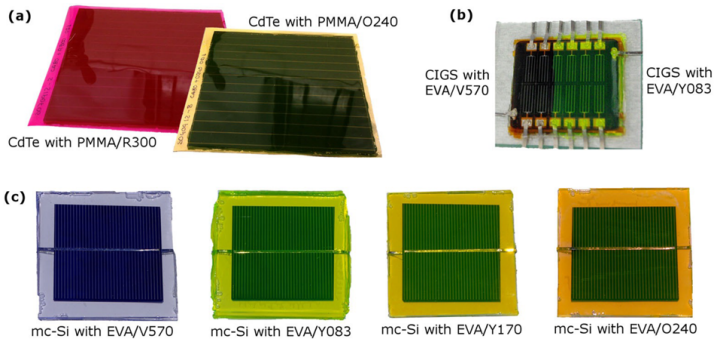

Figure 7. Selection of PV cells coated with different LDS layers: (a) CdTe, (b) CIGS and (c) mc-Si. Lumophores: Lumogen® Violet 570 (V570), Yellow 083 (Y083), Yellow 170 (Y170), Orange 240 (O240), Red 300 (R300). Hosts: poly(methyl methacrylate (PMMA), ethylene vinyl acetate (EVA). Reproduced with permission from reference 95.

QD luminophores have also attracted significant attention in LDS layers for thin film cells. Han *et al.* used CdS and CdSe/ZnS QDs of different sizes to tune the emission color in LDS layers applied to GaAs cells.[114] As GaAs cells have a better short-wavelength response than other thin film technologies, their integration with LDS systems is often overlooked. A PCE increase from 14.48% to 18.05% was achieved for green-emitting CdSe/ZnS QDs applied directly to the cell surface. When QDs are suspended in a host material their LDS efficiency can show concentration dependence, as observed for other luminophores. Hodgson *et al.* characterized the performance of CdS_xSe_{1-x}/ZnS QDs (Φ_{PL} = 51%), doped in PMMA as a function of concentration.[98] Laser beam induced current measurements on the films allowed gains and losses to be imaged and correlated to the QD concentration. A maximum PCE increase of 1.7% was observed at optimum concentration. While high concentrations can cause reabsorption, at moderate concentrations, sufficient to bring the QDs within the Förster radius, FRET can be used to improve light-harvesting efficiency.[123] Commercial QDs Trilite 585 and Trilite 665 (Φ_{PL} = 41%), were deposited onto an InGaP solar cell and subsequently coated with a semiconductor passivation layer. FRET occurred from the passivation layer to the QDs, enabling a two mechanism LDS process, from both direct illumination and FRET. This resulted in an improvement in PCE of 2% giving a maximum PCE of 15.6% compared to the bare cells

(PCE = 13.6%) and illustrates how LDS can be used in conjunction with surface passivation to minimize charge carrier recombination. Another example involved the combination of QD-LDS layers with moth-eyed antireflective coating.[97] Polydimethylsiloxane (PDMS) films were doped with CdZnS/ZnS core-shell QDs (Φ_{PL} > 50%), and nanopatterned using a Si mold to imprint the moth eyed pattern on the PDMS. This moth eyed coating decreased surface reflection to give dual purpose films. A PCE increase of 0.9%, from 27.8% to 28.7%, was observed giving another example of how contemporary LDS layers are viewed as complimentary to other surface treatments. However, LDS layers are not limited to application to the surface of devices. Recently Liao *et al.* deposited CdSe/ZnS QD aggregates (Φ_{PL} = 40%) between the transparent conducting oxide (TCO) anode and a CdS/CIGS p-n junction (PCE = 8.42%) *via* pulsed spray deposition.[124] The aggregates scattered incident light and displaced the absorption closer to the CIGS/CdS interface, where the depletion field is strongest, which consequently increased the average extraction efficiency of the photogenerated carriers, increasing the PCE to 9.34%. The use of internal LDS layers is not limited to QD-based systems. Bouras *et al.* used Nd-doped SnO_2 films as a luminescent TCO layer in CIGS cells.[125] The layers showed efficient energy transfer from the SnO_2 host matrix to the Nd^{3+} dopants, leading to an enhancement of the I_{sc} of the cell. The glass cover slide can also be transformed into an LDS layer by doping with metal ions.[104] Silicate glass slides doped with Ag^+ or Cu^+ by ion exchange were tested as cover slips for GaAs cells.[104] Cu^+ performed better than Ag^+ doped glass, with a 2% increase in maximum power output observed, despite the low Φ_{PL} (0.4%).

AIE luminophores also present a unique opportunity for overcoming concentration-dependent loss mechanisms in LDS. The Dong group investigated the use of TPE-based AIE-gens in PMMA as LDS layers with CdTe cells.[100,126] A family of TPE derivatives exhibiting large Stokes' shifts of over 100 nm and Φ_{PL} of up to 99% was synthesized. An increase in the

I_{sc} of ~5-10% was observed, compared to Lumogen F Yellow 083, which showed a 3-4% increase despite has a similar emission wavelengths.

4.4. Dye-Sensitized Solar Cells

LDS layers can be applied to DSSCs to improve both the spectral response and stability of the device, by inhibiting UV degradation of the dye sensitizer. The first application of LDS to a DSSC was a $LaVO_4:Dy^{3+}$ film functioning both as a UV filter and LDS layer.[127] More recently, Turri, Bongiovanni and *et al.* have demonstrated LDS layers for DSSC based on Eu^{3+} complexes[128] or Lumogen Violet 570[106] doped in fluoropolymeric hosts, which generated an 1.82% (2.68-4.50%) and 1.31% (2.1-3.41%) increase in the PCE, respectively. Long term outdoor stability tests were performed over 2000 h. Notably, the LDS-coated devices showed only 2-7% decrease in PCE with time, whereas uncoated devices decreased by nearly 30% of the initial value. Ahmed *et al.* used plasmonic LDS layers, comprised of PMMA doped with CdSe/ZnS QDS (Φ_{PL} = 71% in solution), to improve the efficiencies of both DSSCs and Si cells.[129] Coupling of the LDS layers to the cells increased the PCE by 2.85-2.98% and 8.4-8.9%, respectively. Hosseini *et al.* applied a dual function LDS-reflective layer onto the bottom of a DSSC.[130] $CaAlSiN_3:Eu^{2+}$ was used as the luminophore (Φ_{PL} = 51%) and through a combination of LDS and back reflection, an increase in PCE of 3.3% to 4.8% was observed. However, despite the potential benefits of LDS layers to DSSCs, there are limited recent examples of innovation in this field.

4.5. Organic Solar Cells

LDS is also an attractive method for improving both the efficiency and stability of OPV. The organic materials used in the photoactive and charge extraction layers can show poor stability to prolonged UV-light exposure, which has limited their commercialization to date.[131] Lanthanide-based luminophores are commonly used in LDS for OPV, including the first example by Xu *et al.* based on $YVO_4:Eu^{3+}/Bi^{3+}$, which increased the stability of the device threefold.[132] More recent work includes the use of nanopatterned LDS layers by direct

nanoimprinting of spin-coated Ln (Eu^{3+} and Tb^{3+}) doped perhydropolysilazane (PHPS) polymer ceramics to give red and green emission respectively (Figure 8).[124] Soft imprint lithography was used to form regular nanocone and nanocylinder patterns on the film surface, which act as scattering centers to increase the photoluminescence intensity compared with the non-patterned analogues. The emission could also be tuned by varying the cone diameter with a red-shift observed with increasing diameter. The nanopatterned films showed both high transparency and water resistance, with a maximum PCE increase from 4.1% to 4.6% observed, along with improved stability. Krebs *et al.* applied commercial tris(hexafluoroacetylacetonate) mono(1,10-phenanthroline)europium (Eu(hfac)(phen)) PMMA inks as LDS layers to OPV cells (PCE 2.79%) by doctor-blading and screen-printing.[133] The bifunctional layers increased the device half-life by 850% for indoor light stability testing and a PCE increase of ~0.25% up to 3.04% was observed. Transition metal complexes such as Ag(POP)(Bphen)(BF_4) (POP = bisphosphinophenyl ether, Bphen = bathophenanthroline) have also been used as direct LDS coatings on OPVs, leading to improved stability over 150 h continuous illumination at 1 sun and a PCE increase from 3.66 to 3.76%.[134]

Contemporary LDS coatings for OPV using more unusual luminophore or host materials have also been reported. Recently, the Zhang group synthesized fluorescent carbon dots (CD) from L-ascorbic acid using (N-(2-aminoethyl)-3-aminopropyl)*tris*-(2-ethoxy) silane as a stabilization and passivation agent, and also as a host material for the CDs.[135] The CD-silane hybrid was converted to a solid through hydrolytic condensation of the silica network due to solvent loss when applied to the cell surface by spin-coating. Upon incorporation into the silane host an increase in Φ_{PL} from 3.8% to 8.6%. An increase in the PCE from 2.85 to 3.18% was observed. A 10-(2-benzothiazolyl)-2,3,6,7-tetrahydro-1,1,7,7-tetramethyl-1 *H*,5*H*,11 *H*-(1) benzopyropyrano(6,7,8-i,j)quinolizin-11-one (C545T) fluorescent molecule doped *tris*(8-quinolinolato) aluminum (C545T:Alq_3) LDS layer (Φ_{PL} = 95%) was applied to an OPV cell, yielding a PCE increase of 0.5% to 3.82%, due to favorable overlap between the C545T

emission and the OPV absorption window.[136] As discussed above for LSCs, silk fibroin can be used as a luminophore host. Prosa *et al.* deposited OPV cells over silk fibroin doped with a stilbene lumophore as a LDS layer.[137] The cells with the silk fibroin showed improved stability (~15% PCE decrease compared with ~35% for reference device) over 70 days in a glove box and afforded an ITO free flexible device.

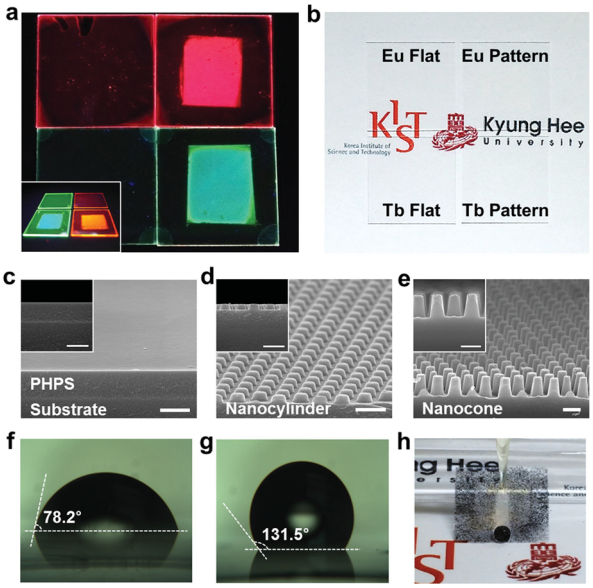

Figure 8. Surface structure and hydrophobicity of nanopatterned LDS layers. (a) Tb^{3+} (green) and Eu^{3+} (red) doped perhydropolysilazane (PHPS) films prepared with or without imprinted nanopatterns on a quartz substrate, under 254 nm illumination. The inset shows the same samples under AM 1.5G illumination through a UV short pass filter (cutoff 400 nm). (b) Photograph of the samples showing high transparency under naturallight. (c–e) Tilted and cross-sectional SEM images of the flat, nanocylinder (diameter = 200 nm, pitch = 400 nm, height = 180 nm) and truncated nanocone (diameter = lower 390 nm/upper 220 nm, pitch = 500 nm, height = 550 nm) samples, respectively. The scale bars indicate 500 nm. Optical microscopy images of water droplets on the surfaces of the nanocylinder patterns (f) prior to and (g) after hydrophobic treatment. (h) A water droplet effectively removed dust particles on the hydrophobic nanopatterns indicating the self-cleaning nature of the surface. Reproduced with permission from reference 124.

4.6 Perovskite Solar Cells

PSCs have rapidly developed since their inception in 2009, with certified cell efficiencies of over 20% achieved to date.[138] The long term stability of PSCs, however, is hindered by a susceptibility to thermal and UV degradation.[139] The first example of LDS applied to PSCs

was by Chander *et al.* who applied a YVO_4/Eu^{3+} nanophosphor by spray deposition to the device surface.[140] The coated PSCs showed higher efficiencies after continuous light soaking, with a PCE increase from 7.42% to 7.93% and improved stability compared to uncoated devices. Interestingly Hou *et al.* demonstrated a method of LDS incorporation into PSCs by doping $ZnGa_2O_4:Eu^{3+}$ into the mesoporous TiO_2 layer.[141] This resulted in a PCE increase of over 3%, from 10.67 to 13.80%, and presents an interesting method of spectral conversion with minimal loss mechanisms. Very recently, Bella *et al*. demonstrated a PSC coated with a Lumogen Violet-fluoropolymer LDS layer on the top side, and an undoped polymer encapsulation coating on the back side of the cell.[142] The coated PSCs showed improved stability over six months compared to the bare devices under continuous UV illumination, with a PCE increase from 17.31 to 18.67%. PSCs with only the Lumogen Violet LDS layer and without the back polymer coating also showed improved stability compared to the bare cells, with efficiency losses only occurring after 75 days continuous illumination in an inert atmosphere. This result indicates that the role of the LDS layer in reducing UV degradation is critical. While examples of LDS for PSCs are limited to date, the field is highly dynamic, and this will certainly change in the near future.

5. Upconversion

5.1 Working principle and figures-of-merit

It is counterintuitive that low energy excitation can give rise to a higher energy emission, however upconversion is a promising method to harvest sub-bandgap photons.[3] UC is a nonlinear anti-Stokes process which relies on the absorption of two or more sub-bandgap photons which can undergo upconversion *via* a variety of mechanisms, the most common of which are excited state absorption (ESA) and energy transfer upconversion (ETU).[3] ESA involves sequential absorption of two (or more) photons by a ion/molecule already in an excited state, and results in further excitation of that species to a higher energy state. In ETU, two photons excite neighboring ions/molecules to a metastable energy level and energy is

exchanged through dipole-dipole interactions to promote one species to a higher energy level and relax the other one.[3] In both cases, radiative relaxation of the higher excited energy level to the ground state leads to the emission of the desired higher-energy photon. Other less common mechanisms for UC include photon avalanche (PA),[143] energy-mediated migration upconversion (EMU)[144] and for organic materials in particular triplet-triplet annihilation (TTA).[6,145,146]

The efficiency of upconversion is characterized by the quantum yield (UCQY). The *internal* UCQY is defined as the ratio of flux of emitted UC photons (ϕ_{UC}) to the photon flux absorbed by the sample (ϕ_{abs}):[6]

$$internal\ UCQY = \frac{\phi_{UC}}{\phi_{abs}} \tag{4}$$

Since at least two photons must be absorbed in order to create one emitted photon of higher energy than the individual absorbed ones, the internal UCQY is limited to ≤50%. The *external* UCQY is also commonly reported:

$$external\ UCQY = \frac{\phi_{UC}}{\phi_{in}} \tag{5}$$

where ϕ_{in} is the incident photon flux on the sample. Since upconversion is a nonlinear processes, the intensity of the UC photoluminescence shows power law dependence on the irradiance of excitation, given by an exponent n_{ph}, the number of photons that must be absorbed to excite the UC process.[6] At high irradiances, the UC process saturates and the UCQY levels off to a constant value. To facilitate comparison of different UC materials (and their performance in different PV devices), the normalized UCQY has been proposed:

$$normalized\ UCQY = \frac{UCQY}{I_R} \tag{6}$$

where I_R is the irradiance of the excitation source. This normalization can be applied to both internal and external UCQY, as well as the EQE of the PV device.[6] However, in PV devices, the UC performance is most typically reported in terms of the enhancement in the PCE.

Until recently, upconverting materials were limited to those containing rare-earth ions such as Er^{3+}, Tm^{3+} and Ho^{3+}, which are characterized by a series of well-defined ladder-like energy levels originating from partial occupancy of the 4*f* shell.[3] Since direct excitation of these ions is inefficient, they are commonly used in conjunction with Yb^{3+} as a sensitizer, due its large absorption cross-section in the NIR region.[3] Typical host materials are sodium rare-earth tetrafluorides [147,148], or oxysulfides[149,150] due to their low phonon energy, high thermal stability, high transparency in the NIR range and high refractive index. As these UC systems are well-established, the following sections will focus on the emerging materials in this field: upconversion nanocrystals (UCNC) and TTA upconverters.

5.2 Upconversion Nanocrystals

UCNCs are made from traditional upconversion materials converted into nanomaterial architectures (*i.e.* individual crystals, ~15-500 nm in size). While UCNCs offer more variety in the modes of incorporation into PV cells, their performance is often limited by surface quenching resulting in lower UCQY values compared to their bulk counterparts.[151] Contemporary work has focused on overcoming this limitation in device formats. The limited absorption range of DSSCs makes them attractive candidates for integration with UC.[152,153] Recent work has utilized one and two-dimensional nanomaterials to improve both conductivity and spectral response of the photoelectrode layers in DSSCs. Bai *et al.* applied electrospun CeO_2:Er^{3+},Yb^{3+} nanofibers to the photoelectrode layer of a DSSC using di-tetrabutylammonium *cis*-bis(isothiocyanato)bis(2,2′-bipyridyl-4,4′-dicarboxylato)ruthenium(II) (N719, dyesol) as the sensitizer by spin-coating.[152] A 14% enhancement in the PCE was obtained from 5.79% for the uncoated cell to 6.66%. Interestingly, DSSCs incorporating pure CeO_2 nanowires alone also showed increased current density compared to the reference cell, although lower than

observed for the Er^{3+},Yb^{3+} doped analogues. This enhancement was attributed to a combination of increased absorption due to the presence of CeO_2 scattering centers, coupled with superior harvesting of low energy photons due to the UC effect. The bifunctionality of UCNC layers was also recently demonstrated by Wu *et al.* who designed reduced graphene oxide (rGO) NaYF4:Yb^{3+},Er^{3+} UCNC composites for incorporation into DSSCs to improve conductivity (Figure 9).[147] The composites were prepared using a solvothermal route and subsequently screen-printed onto the TiO_2 layer of the DSSC. A comparison of pure UCNCs of different sizes and their non-chemically bonded UCNC/rGO composites was performed. A relative improvement in the PCE from 5.63% to 6.20% was observed for DSSCs incorporating nanometer-sized pure UCNCs, whereas a decrease was measured for micometer-sized particles and the UCNC/rGO composites. This thus demonstrated the use of UCNCs to both improve conductivity and spectral response of PV cells and that UCNC can outperform their bulk equivalents in certain architectures.

In both of the above cases the UCNC was applied to the photoanode after the TiO_2 mesoporous layer was applied. This is the most common method of incorporation of UCNCs into DSSCs, as it allows for a large surface area to maximize absorption, and most devices prepared in this way exhibit similar enhancements in the PCE. For example, Gd_2O_3:Ho^{3+},Yb^{3+} nanoparticles prepared by homogeneous precipitation method delivered a relative improvement of 6.7 to 7.4% PCE following their application to the TiO_2 layer of a DSSC.[154] However, this architecture is not a strict requirement. Chander *et al.* obtained an increase in the PCE of 0.88% (7.14% to 8.02%) by directly mixing core-shell $NaYF_4$:Yb^{3+},Er^{3+}/$NaYF_4$ NPs with TiO_2, thus embedding the nanoparticles in the mesostructured layer.[153] The core-shell NPs were synthesized by thermal decomposition and mixed with TiO_2 paste before application by doctor-blading. Yu *et al.* recently investigated this method of incorporation using YbF_3:Ho^{3+}/TiO_2 nanoheterostructures and used surface photovoltage and transient photovoltage techniques to gain insight into the charge transport properties within the layer.[155] An enhancement in the

overall PCE from 6.5% to 8.0% and a 19% improvement in the photocurrent was obtained compared to the bare TiO_2 devices and a mechanism for the NIR-harvesting in UC DSSCs was proposed, which involved a combination of partial electron injection from the YbF_3:Ho^{3+} to the TiO_2 and a luminescence-mediated energy transfer from the UC to the N719 dye sensitizer.

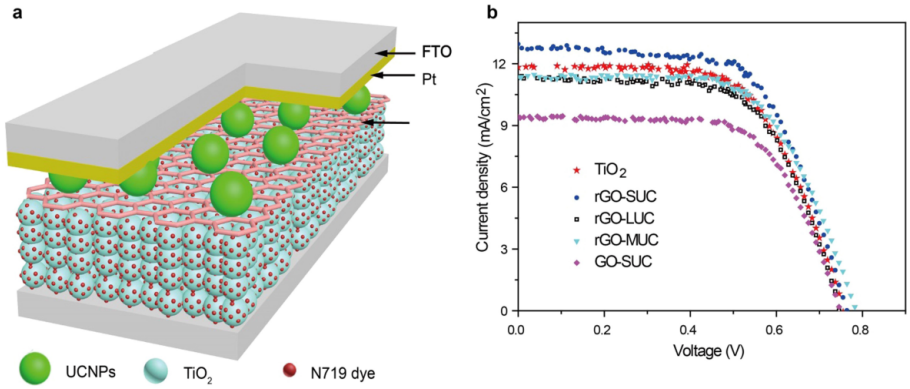

Figure 9. (a) Schematic structure of a dye-sensitized solar cell (DSSC) containing graphene oxide (GO)-upconverting nanocrystal (UCNP)composites (pink hexagons). (b) Photocurrent–voltage (I–V) curves of DSSCs with different GO–UCNP composites under AM 1.5 G irradiation. FTO = fluorine-doped tin oxide; rGO = reduced graphene oxide; SUC/LUC = small, or large unconverting nanocrystal; MUC = physically mixed UCNP rGO composites. Reproduced with permission from reference 147 (DOI: 10.1088/0957-4484/27/34/345703).

Since PSCs have an analogous device architecture to DSSCs, a similar method of incorporation is possible, and UCNCs have been used both in and as the mesostructured layer. The first example of UC for PSCs was by Chen *et al*. who used a single crystal $LiYF_4$:Yb^{3+}, Er^{3+} layer with an internal UCQY of 5.72%, coated on top of the PSC in an external architecture.[148] The PCE was enhanced from 11% to 11.9% under irradiation with simulated sunlight by 7−8 solar constants (730 mW/cm^2). Shortly after publication of this paper, He *et al*. reported the use of $NaYF_4$:Yb^{3+},Er^{3+} UCNCs as a replacement for the conventional TiO_2 mesostructured layer in PSCs.[156] The UCNCs were crafted within a poly(acrylic acid)-*block*-poly(ethylene oxide) (PAA-*b*-PEO) nanoreactor and spin-coated onto the TiO_2 blocking layer, which was subsequently ozone-etched to give a porous UCNC layer. An increase in the PCE from 16.83% to 17.78% was observed for the champion pure UCNC devices, compared to the conventional TiO_2 analogues. More recently, the Jang group used hexagonal β-$NaYF_4$:Yb^{3+},

Er^{3+} nanoprisms in PSCs for NIR-harvesting through their incorporation into the TiO_2 layer.[157] These doped devices displayed UC under 980 nm illumination and showed increased PCE under AM 1.5G from 14.05% to 15.98%.

While UCNCs are well-studied in conjunction with DSSCs and PSCs, there have been very few reports of their direct application with other PV cell types. In this context, efforts have focused instead improving control over the synthesis and optical properties of UCNCs, with the aim of tuning their compatibility with other PV classes. Wang *et al.* synthesized triple-doped ($Yb^{3+}/Er^{3+}/Tm^{3+}$) $KMnF_3$ nanocubes (~250 nm) through a hydrothermal route.[158] The nanocubes simultaneously exhibited four-color (blue, green, red and NIR) upconversion emissions under a single 980 nm laser excitation. This emission is useful for PV cells which absorb broadly, such as Si PV. Conversely, Shao *et al.* used a variety of multishell UCNPs consisting of $NaYF_4$ doped with varying amounts of Ln^{3+} ions organized into core-shell structures (Eu^{3+} core, Ho^{3+} and Tm^{3+} shells) with $NaYF_4$ shells as spacers. These core shell structures show wavelength-dependent emission related to the separation (or not) of the Ln^{3+} doped layers, enabling coverage of a broad spectral range in the NIR region.[159] Other work has focused on improving the UCQY. Wisser *et al.* removed Y^{3+} ions from the $NaYF_4$ host, and replaced them with Gd^{3+} and Lu^{3+}, causing contraction of lattice.[160] A 1.6 times enhancement of the UCQY up to 0.074% was observed when compared with the reference host due to distorted symmetry allowing additional Ln^{3+} coordination. Chen *et al.* used a carboxylic acid treated commercial IR absorbing dye (IR-783) sensitizer bound to $NaYF_4/Ln^{3+}$ UCNCs to improve UCQY by energy cascade upconversion (ECU).[161] Incident light was efficiently harvested by broad absorption of the IR dye, which underwent nonradiative energy transfer to the UCNCs delivering a UCQY of 4.8%.

5.3 Triplet-Triplet Annihilation

Upconversion through TTA is the most common mechanism for organic (or organometallic) materials, and typically involves a different sensitizer and annihilator species.[145,146] The basic

mechanism is analogous to that of ETU, with the addition of a few extra steps (Figure 10). The sensitizer species absorbs low-energy photons, leading to population of an excited singlet state $S_{1(S)}$, which subsequently relaxes to the lower energy triplet state, $T_{1(S)}$, by ISC. Triplet–triplet energy transfer *via* electron exchange excites neighboring emitter molecules to their lowest triplet state $T_{1(E)}$. Collisional encounters between two long-lived $T_{1(E)}$ states may then result in triplet–triplet annihilation, leading to population of one higher energy singlet state $S_{1(E)}$ in one of the emitter species. Radiative relaxation of this excited state generates a single, high energy, upconverted photon. Several recent reviews have provided an excellent overview of solution-based TTA systems and Table 3 summarizes the figure of merit for some representative TTA-UC systems in conjunction with various PV devices.[145,146]

Table 3. The performance of TTA-UC layers upon application to different PV devices according to the current enhancement per cm^2, per solar concentration factor (FOM).

Cell Type	Sensitizer (S)	Emitter (E)	λ_{abs} (E),(S) (nm)	λ_{em} (nm)	FOM ($mA/cm^2/\Theta^2$)	Reference
a-Si	PQ_4Pd	Rubrene	400-500, 650-700	560	2.8×10^{-5} [a]	169
a-Si	PQ_4PdNA	Rubrene	400-500, 650-750	560	1.4×10^{-4} [a]	169
DSSC	PQ_4PdNA	Rubrene	400-500, 650-750	560	2.5×10^{-4}	167
P3HT:ICBA	PQ_4PdNA	Rubrene	400-500, 650-750	560	1.60×10^{-4}	168
PCDTBT:$PC_{71}PM$	PQ_4PdNA	Rubrene	400-500, 650-750	560	1.54×10^{-4}	168
(n) a-SiH/ (i) a-Si:H/ (p) µc-SiO_x:H	PQ_4PdNA	Rubrene	400-500, 650-750	560	7.63×10^{-4}	168
a-Si	PQ_4PdNA	Rubrene/BPEA	400-500, 650-750	450-650	2.4×10^{-3}	170
DSSC	PQ_4PdNA	Rubrene/BPEA	400-500, 650-750	450-650	4.5×10^{-3}	170

PQ_4Pd/PQ_4PdNA - tetrakisquinoxalinoporphyrin derivatives; PCDTBT - poly[[9-(1-octylnonyl)-9*H*-carbazole-2,7-diyl]-2,5-thiophenediyl-2,1,3-benzothiadia-zole-4,7-diyl-2,5-thiophenediyl]; $PC_{71}PM$ - [6,6]-phenyl C_{71}butyric acid methyl ester.

Since absorption is an allowed process for the sensitizer, high absorption cross-sections can be obtained, which is an improvement on lanthanide upconverters. However, organic

materials exhibit limited photo- and chemical stability and TTA is a diffusion-controlled process, factors which represent major barriers for TTA in the context of its application in solid-state PV devices. To overcome this significant challenge, current research is directed towards the incorporation of TTA-UC materials within solid or *quasi*-solid matrices, such as polymers or gels. In polymer matrices, the efficiency of TTA-UC is significantly enhanced when polymers with a low glass transition temperature (T_g) are used. For example, Singh-Rachford *et al.* demonstrated that the TTA-UC efficiency in ethyleneoxide and epichlorohydrin co-polymers and several commercial polyurethanes was significantly enhanced at temperatures below T_g, due to increased diffusion of the sensitizer and emitter species.[162] Meinardi *et al.* also reported efficient TTA-UC in polyacrylate elastomers of different sidechain lengths doped with a platinum(II) octaetyl-porphyrin (PtOEP) and 9,10-diphenylanthracene (DPA) and sensitizer-emitter pair, with the UC efficiency being directly related to the diffusion length and T_g of the elastomers.[163] Emissive conjugated poly(fluorenes) doped with metal(II) octaetyl porphyrins have also been investigated as dual host-emitter upconversion layers and show temperature dependent photoluminescence.[164]

Some of the most promising recent results have been obtained with quasi-solid gels. Duan *et al.* observed TTA in *N,N*-bis(octadecyl)-*L*-boc-glutamic diamide organogel matrices through the spontaneous accumulation of donor and acceptor molecules in the gel nanofibers, which are stabilized by extended hydrogen-bond networks (Figure 10).[165] They investigated a large variety of donor and acceptor TTA systems, which enabled near IR-to-yellow, red-to-cyan, green-to-blue, and blue-to-UV wavelength conversions. Due to scattering from the gel it proved difficult to measure the UCQY of the TTA systems, however the absolute QY could be determined and values up to 3.5% were obtained. The gel also acts as an oxygen barrier, preventing quenching of the triplet excited state. Sripathy *et al.* researched organogels prepared from a 1,3:2,4-*bis*(3,4-dimethylbenzylidene) sorbitol gelator in tetralin as the solvent and doped with palladium tetraphenylporphyrin (PdTPP) and 10-diphenylanthracene (DPA), as the

sensitizer and emitter TTA molecules, respectively.[166] A UCQY of 0.07 was determined under one-sun irradiation, despite the high viscosity of the tetralin solvent. The same group have pioneered the application of TTA-UC layers to several different PV cell types including a-Si, DSSCs and OPVs.[167–170] In these devices, a liquid phase TTA UC layer was enclosed in a cavity or cuvette placed below the PV cell. The improvement in the cell efficiency achieved through the addition of the TTA-UC layer was assessed using a figure of merit whereby the current enhancement is determined per cm^2, per solar concentration factor (Θ). The a-Si and DSSC cells achieved a maximum increase in current of 2.4×10^{-3} $mAcm^{-2}\Theta^{-2}$ and 4.5×10^{-3} $mAcm^{-2}\Theta^{-2}$, respectively when a dual emitter TTA system was applied.[170] The same approach applied to OPV cells had more moderate success with a maximum increase in current of 1.6×10^{-4} $mAcm^{-2}\Theta^{-2}$ achieved for a cell based on poly(3-hexylthiophene-2,5-diyl (P3HT) and 1′,1″,4′,4″-tetrahydro-di[1,4]methanonaphthaleno[5,6]fullerene-C_{60} (ICBA).[168]

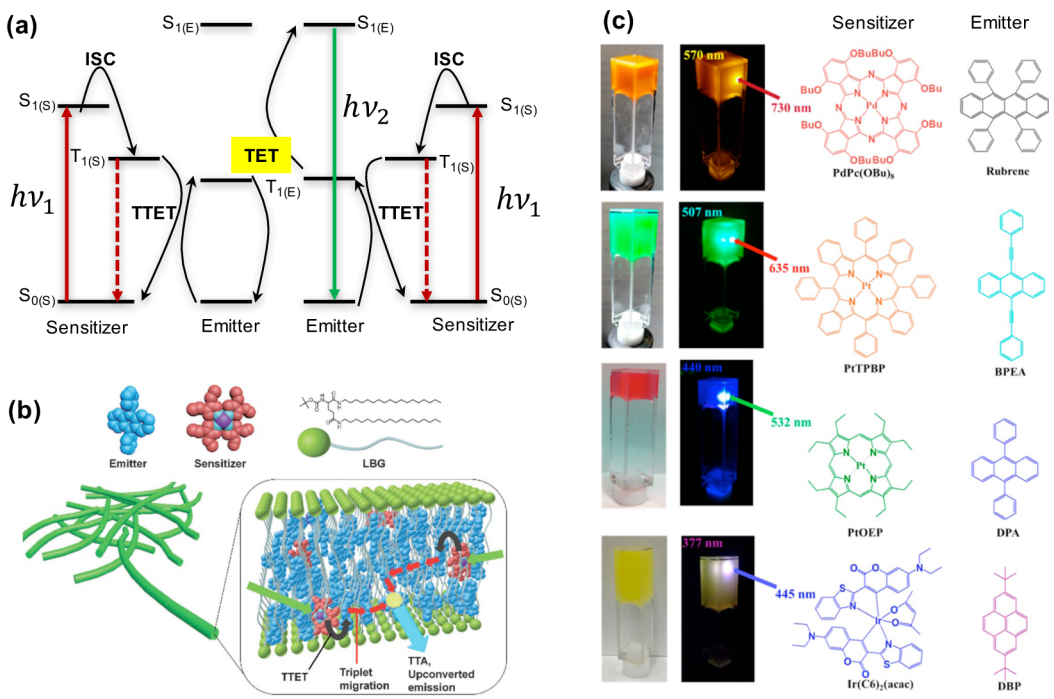

Figure 10. Triplet-triplet annihilation upconversion (TTA-UC) in supramolecular gel hosts. (a) Energy level diagram of the process leading to TTA upconversion. The sensitizer (S) absorbs low-energy photons ($h\nu_1$), leading to population of an excited singlet state $S_{1(S)}$, which subsequently relaxes to the lower energy triplet state, $T_{1(S)}$, by

intersystem crossing (ISC). Triplet–triplet energy transfer (TTET) excites neighboring emitter molecules to their lowest triplet state $T_{1(E)}$. Collisional encounters between two long-lived $T_{1(E)}$ states may then result in TTA, leading to population of one higher energy singlet state $S_{1(E)}$ in one of the emitter species. Radiative relaxation of this excited state generates a single, high energy, upconverted photon ($h\nu_2$). (b) Sensitizer (red) and acceptor (blue) molecules are incorporated in *N,N′*-bis(octadecyl)-L-boc-glutamic diamide (LBG) gel fibers as extended domains. TTA occurs via the process described above. (c) Photographs of the LBP cogels in air-saturated dimethylformamide and corresponding chemical structures of the sensitizer and acceptor pairs used in each case. Adapted with permission from P. Duan, N. Yanai, H. Nagatomi, N. Kimizuka, *J. Am. Chem. Soc.* **2015**, *137*, 1887. Copyright 2015 American Chemical Society.

TTA sensitizer and emitter molecules are limited to a handful of classes. The requirements for effective TTA are fast donor ISC, efficient donor-acceptor triplet-triplet energy transfer, fast acceptor TTA and acceptor fluorescence.[145] Quantum dots and metalloporphyrins are commonly used as sensitizers, while anthracene derivatives are typical emitters.[145,146,171,172] The Tang group investigated a TTA system based on CdSe QD sensitizers functionalized with 9-anthracene carboxylic acid (9-ACA) as a transmitter, and a DPA acceptor.[173] They demonstrated that UCQY has a quadratic to linear dependence on the QD concentration, and the upconversion efficiency correlates positively with the surface coverage of the 9-ACA transmitter and the emission quantum yield of the sensitizer, but negatively with particle size. A maximum UCQY of 7.7% was achieved for 2.7 nm QDs with PLQY of 11%.

Since the efficiency of TTA-UC is collision-dependent, the arrangement of sensitizer and emitter molecules within a host matrix and with respect to each other is critical. The theoretical model reported by Zimmerman *et al*. predicted that a twofold in the upconversion efficiency can be obtained if the sensitizer species are distributed as clusters within a homogeneous dispersion of isolated emitter molecules, compared to a random distribution of both species.[174] Zhang and coworkers also recently showed that the spatial distribution of emitters critically influenced the UC efficiency in poly(9-anthrylmethyl methacrylate) emitter copolymers doped with PtOEP as a sensitizer.[175] For most luminophores, emission is typically

isotropic; however there are a number of advantages for directed emission as discussed above in relation to LSCs. Börjesson *et al.* recently used liquid crystals to achieve anisotropic UC emission.[172] Palladium(II)octaethylporphyrin (PdOEP) and anthracene derivatives used as a sensitizer/emitter combination were mixed with a liquid crystalline matrix and sealed in a custom UC cell showing UCQY up to 0.76%. The anthracene derivatives display orientational order, while the porphyrin sensitizer absorbs light from all directions. The emission direction and intensity could thus be controlled through the application of a voltage to switch the host between nematic and ordered LC phases, which subsequently changed the orientation of the doped luminophores. Very recently Hagstrom *et al.* have reported dual sensitizer TTA-UC systems which utilize two sensitizer metalloporphyrins (PtOEP and PdTPBP) and perylene as an acceptor, all immobilized in a polyurethane film.[176] They showed that a "multijunction" architecture comprised of two individual films containing either PtOEP or PdTPBP sensitizers stacked on top on each either achieved strong broadband light absorption and improved TTA-UC efficiency compared to a single film comntaining a blend of the the two senstizers at comparable concentration.

To date, there has been only one example of a functional solid-state TTA UC layer without a host material.[171] PbS nanocrystal sensitizers were cast as thin films on glass and coated with a thermally-evaporated film of rubrene doped with 0.5 vol% of dibenzotetraphenyl-periflanthene (DBP). Rubrene has a favorable triplet excited state energy for sensitization by the PbS, and subsequently undergoes TTA, followed by a host-guest interaction to generate a singlet excited state on the DBP. Upconversion at wavelengths greater than 1000 nm was observed, which is uncommon for TTA systems.

6. Outlook and Perspectives

As illustrated in this report, spectral converters present a significant opportunity for improving the efficiency of PV cells. If deployed correctly, spectral converters may help to accelerate the proliferation and uptake of solar technologies – an urgent need if global commitments to

reducing CO_2 emissions are to be met. However, there are still many barriers to be overcome before spectral converters are likely to reach the market place.

For LSCs, there continues to be an over-dependence on well-characterized materials and a lack of consistency in the experimental determination and reporting of optical efficiencies makes it extremely challenging to benchmark performance. There is a clear need to explore new materials – particularly as waveguides – to overcome the current bottleneck in the optical efficiency. Elegant approaches to control the luminophore orientation and placement within the waveguide have been reported and this strategy must be investigated further if reabsorption losses are to be fully mitigated. New luminophores exhibiting large Stokes' shifts or orthogonal absorption and emission transition dipoles must be designed to further address this challenge. One potential hurdle to overcome is acceptance of their unmistakable appearance – LSCs are bright, colorful and indiscrete! However, a recent study using a red LSC as a power-generating window in an office environment was judged favorably by volunteer participants when compared to a normal, clear glass window,[177] suggesting that market acceptance is not a key barrier to commercialization of this technology.

Since LDS layers are primarily integrated as a coating on the surface of a PV cell, they offer considerable scope for the addition of multifunctionality. Examples where the LDS coating also exhibits barrier properties, hydrophobicity and even antireflectivity have recently been reported. However, this is non-trivial, particularly in the case of superhydrophobic surfaces which often exhibit a high surface roughness – an intrinsic source of scattering defects! However, this challenge should be tackled, since a dual light-harvesting, water-repellant encapsulation layer is particularly attractive prospect for improving both the efficiency and stability of hydroscopic perovskite cells. The integration of the LDS layer within the PV cell itself is another intriguing possibility that has been relatively unexplored. Given the potential to minimize interface losses, this approach should not be overlooked.

The low UCQY exhibited by rare-earth nanocrystalline upconverters continues to put them at a disadvantage to their bulk phase counterparts. Surface passivation and coating methods appear to be a promising strategy to overcome this limitation. However, there is still much to be done in terms of developing reproducible – and scalable - synthetic routes to highly emissive, defect-free nanocrystals and in-depth quantitative studies are required to fully understand the effect of quenching by defects. For TTA upconverters, the primary challenge is the translation of efficient solution-based systems to the solid-state. Soft materials such as gels and polymers appear to provide a viable compromise to the need for a robust yet mobile host medium and further research in this field, particular in the context of supramolecular assembly to control luminophore placement, is likely to generate exciting results.

The LSC, LDS and UC fields all suffer from discrepancies in the experimental determination and reporting of the spectral conversion performance. It is clear that a coordinated effort is required from community to define measurement protocols, including a more rigorous approach to the reporting of all relevant experimental information. The sister photovoltaic community has benefitted enormously from the introduction of standard test conditions and independent laboratories to verify device performance. The availability of more reliable data would make it easier to more clearly pinpoint the direction for targeted spectral conversion materials and increased transparency would accelerate progression in the field.

Although not discussed in detail here, quantum cutting could potentially overcome the efficiency limitations of LDS and LSCs in their current architectures. Since QC requires that the incident light possesses an energy of at least twice the E_g of the solar cell,[1] it is a more effective mechanism for small E_g devices, as more incident photons will have sufficient energy to initiate the process. While purely theoretical calculations have suggested that QC could improve the efficiency of single junction PV cells to 39.63%,[178] a more recent study by Van der Kolk *et al.* investigated the efficiency limits of QC layers for a variety of commercial PV cells taking practical conditions into account and predicted a more modest PCE increase of 3%

for c-Si cells, up to a maximum PCE increase of 11% for low bandgap (E_g = 0.7 eV) GaSb cells.[179] The luminophores traditionally used are based on lanthanide pairs of Ln^{3+}-Yb^{3+} (Ln^{3+} = Tb^{3+}, Tm^{3+}, Pr^{3+}, Er^{3+}, Ho^{3+}), which undergo QC by either sequential emission from one emissive center or energy transfer between two emissive centers.[3] Such materials have shown a high Φ_{PL} of up to 195% and tuning of the Ln^{3+} donor to Ce^{3+} or Eu^{2+} and doping into inorganic hosts such as borate or silicate glasses can achieve the broad absorption cross-sections required[3,180] Recent practical examples of Tb^{3+}/Yb^{3+}QC layers applied to c-Si and GaP cells have demonstrated a PCE enhancement from 6.98% to 7.47% and from 0.691% to 0.699%, respectively.[181] As such, there is clearly some way to go before the significant enhancement in PCE predicted for QC materials is achieved. Materials innovation in this area will likely stem from the diversification of the current limited library of suitable QC luminophores, which is clearly the bottleneck at present. Promising results have recently been reported utilizing PbSe, PbS, PbTe, CdSe and Si nanocrystals as QC layers due to the multiple exciton generation properties that they exhibit.[3,182] In particular, Si nanocrystals have been shown by to undergo space separated quantum cutting and step-like quantum yield enhancement.[183,184] QC Eu^{3+} doped $NaGdF_4$ nanocrystals have also recently been applied to DSSCs and a PCE increase from 8.94 to 9.34% was observed.

Ultimately, spectral converters need to be integrated into a single luminescent solar device, containing both a DS/QC layer and UC layer, to yield a high performance solar cell. While promising steps have been made, this device has yet to be fully realized. This is potentially because most studies have focused on silicon solar cells, whose architecture and performance is firmly entrenched. The strategic development of spectral converters alongside newer, emerging photovoltaic technologies such as perovskite and organic solar cells, perhaps presents the best hope for commercial uptake, and has the potential to deliver highest efficiency gains.

Acknowledgements

This work was supported by the Science Foundation Ireland under Grant No. 12/IP/1608. The authors would like to thank Dr. Joel Troughton of SPECIFIC – College of Engineering, Swansea University for providing the EQE data used in Figure 2.

References

[1] B. S. Richards, *Sol. Energy Mater. Sol. Cells* **2006**, *90*, 2329.
[2] W. Shockley, H. J. Queisser, *J. Appl. Phys.* **1961**, *32*, 510.
[3] X. Huang, S. Han, W. Huang, X. Liu, *Chem. Soc. Rev.* **2013**, *42*, 173.
[4] E. Klampaftis, D. Ross, K. R. McIntosh, B. S. Richards, *Sol. Energy Mater. Sol. Cells* **2009**, *93*, 1182.
[5] M. G. Debije, P. P. C. Verbunt, *Adv. Energy Mater.* **2012**, *2*, 12.
[6] J. C. Goldschmidt, S. Fischer, *Adv. Opt. Mater.* **2015**, *3*, 510.
[7] M. A. Green, K. Emery, Y. Hishikawa, W. Warta, E. D. Dunlop, *Prog. Photovoltaics Res. Appl.* **2016**, *24*, 905.
[8] J. Zhao, Y. Li, G. Yang, K. Jiang, H. Lin, H. Ade, W. Ma, H. Yan, *Nat. Energy* **2016**, *1*, 15027.
[9] S. Mathew, A. Yella, P. Gao, R. Humphry-Baker, B. F. E. Curchod, N. Ashari-Astani, I. Tavernelli, U. Rothlisberger, M. K. Nazeeruddin, M. Grätzel, *Nat. Chem.* **2014**, *6*, 242.
[10] Q. Y. Zhang, X. Y. Huang, *Prog. Mater. Sci.* **2010**, *55*, 353.
[11] D. Chen, Y. Wang, M. Hong, *Nano Energy* **2012**, *1*, 73.
[12] T. Trupke, M. A. Green, P. Würfel, *J. Appl. Phys.* **2002**, *92*, 4117.
[13] T. Trupke, M. A. Green, P. Würfel, *J. Appl. Phys.* **2002**, *92*, 1668.
[14] S. F. H. Correia, P. P. Lima, E. Pecoraro, S. J. L. Ribeiro, P. S. André, R. A. S. Ferreira, L. D. Carlos, *Prog. Photovoltaics Res. Appl.* **2016**, *24*, 1178.
[15] F. Purcell-Milton, Y. K. Gun'ko, *J. Mater. Chem.* **2012**, *22*, 16687.
[16] M. G. Debije, W. Dekkers, *J. Renew. Sustain. Energy* **2012**, *4*, 13103.
[17] W. G. J. H. M. van Sark, K. W. J. Barnham, L. H. Slooff, A. J. Chatten, A. Büchtemann, A. Meyer, S. J. McCormack, R. Koole, D. J. Farrell, R. Bose, E. E. Bende, A. R. Burgers, T. Budel, J. Quilitz, M. Kennedy, T. Meyer, C. D. M. Donegá, A. Meijerink, D. Vanmaekelbergh, *Opt. Express* **2008**, *16*, 21773.
[18] S. F. H. Correia, V. de Zea Bermudez, S. J. L. Ribeiro, P. S. André, R. A. S. Ferreira, L. D. Carlos, *J. Mater. Chem. A* **2014**, *2*, 5580.
[19] A. Kaniyoor, B. McKenna, S. Comby, R. C. Evans, *Adv. Opt. Mater.* **2016**, *4*, 444.
[20] J. B. Birks, *Photophysics of Aromatic Molecules*, Wiley, **1970**.
[21] J.-C. G. Bünzli, A.-S. Chauvin, *Lanthanides in Solar Energy Conversion*, Elsevier Science B.V., **2014**.
[22] J. C. G. Bunzli, C. Piguet, *Chem. Soc. Rev.* **2005**, *34*, 1048.
[23] R. C. Evans, P. Douglas, C. J. Winscom, *Coord. Chem. Rev.* **2006**, *250*, 2093.
[24] O. Moudam, B. C. Rowan, M. Alamiry, P. Richardson, B. S. Richards, A. C. Jones, N. Robertson, *Chem. Commun.* **2009**, *29*, 6649.
[25] M. J. Currie, J. K. Mapel, T. D. Heidel, S. Goffri, M. A. Baldo, *Science* **2008**, *321*, 226.
[26] B. Mahler, P. Spinicelli, S. Buil, X. Quelin, J.-P. Hermier, B. Dubertret, *Nat. Mater.* **2008**, *7*, 659.
[27] K. Yu, J. Ouyang, Y. Zhang, H. T. Tung, S. Lin, R. A. L. Nagelkerke, D. Kingston, X. Wu, D. M. Leek, D. Wilkinson, C. Li, I. G. Chen, Y. Tao, *ACS Appl. Mater. Interfaces* **2011**, *3*, 1511.
[28] W. Zhang, Y. Li, H. Zhang, X. Zhou, X. Zhong, *Inorg. Chem.* **2011**, *50*, 10432.

[29] Y. Zhao, R. R. Lunt, *Adv. Energy Mater.* **2013**, *3*, 1143.
[30] F. Meinardi, A. Colombo, K. A. Velizhanin, R. Simonutti, M. Lorenzon, L. Beverina, R. Viswanatha, V. I. Klimov, S. Brovelli, *Nat. Photonics* **2014**, *8*, 392.
[31] Z. Krumer, S. J. Pera, R. J. A. van Dijk-Moes, Y. Zhao, A. F. P. de Brouwer, E. Groeneveld, W. G. J. H. M. van Sark, R. E. I. Schropp, C. de Mello Donegá, *Sol. Energy Mater. Sol. Cells* **2013**, *111*, 57.
[32] L. R. Bradshaw, K. E. Knowles, S. McDowall, D. R. Gamelin, *Nano Lett.* **2015**, *15*, 1315.
[33] I. Coropceanu, M. G. Bawendi, *Nano Lett.* **2014**, *14*, 4097.
[34] Y. Zhou, D. Benetti, Z. Fan, H. Zhao, D. Ma, A. O. Govorov, A. Vomiero, F. Rosei, *Adv. Energy Mater.* **2016**, *6*, 1501913.
[35] C. S. Erickson, L. R. Bradshaw, S. McDowall, J. D. Gilbertson, D. R. Gamelin, D. L. Patrick, *ACS Nano* **2014**, *8*, 3461.
[36] O. O. Matvienko, Y. N. Savin, A. S. Kryzhanovska, O. M. Vovk, M. V. Dobrotvorska, N. V. Pogorelova, V. V. Vashchenko, *Thin Solid Films* **2013**, *537*, 226.
[37] F. Meinardi, H. McDaniel, F. Carulli, A. Colombo, K. A. Velizhanin, N. S. Makarov, R. Simonutti, V. I. Klimov, S. Brovelli, *Nat. Nanotechnol.* **2015**, *10*, 878.
[38] K. M. Tsoi, Q. Dai, B. A. Alman, W. C. W. Chan, *Acc. Chem. Res.* **2013**, *46*, 662.
[39] S. Y. Lim, W. Shen, Z. Gao, *Chem. Soc. Rev.* **2015**, *44*, 362.
[40] C. M. Gonzalez, J. G. C. Veinot, *J. Mater. Chem. C* **2016**, *4*, 4836.
[41] J. Mei, N. L. C. Leung, R. T. K. Kwok, J. W. Y. Lam, B. Z. Tang, *Chem. Rev.* **2015**, *115*, 11718.
[42] Y. Hong, J. W. Y. Lam, B. Z. Tang, *Chem. Soc. Rev.* **2011**, *40*, 5361.
[43] J. Mei, Y. Hong, J. W. Y. Lam, A. Qin, Y. Tang, B. Z. Tang, *Adv. Mater.* **2014**, *26*, 5429.
[44] J. L. Banal, J. M. White, K. P. Ghiggino, W. W. H. Wong, *Sci. Rep.* **2014**, *4*, 4635.
[45] J. L. Banal, K. P. Ghiggino, W. W. H. Wong, *Phys. Chem. Chem. Phys.* **2014**, *16*, 25358.
[46] J. L. Banal, J. M. White, T. W. Lam, A. W. Blakers, K. P. Ghiggino, W. W. H. Wong, *Adv. Energy Mater.* **2015**, *5*, 1500818.
[47] C. Shi, Z. Guo, Y. Yan, S. Zhu, Y. Xie, Y. S. Zhao, W. Zhu, H. Tian, *ACS Appl. Mater. Interfaces* **2013**, *5*, 192.
[48] X. Gu, J. Yao, G. Zhang, Y. Yan, C. Zhang, Q. Peng, Q. Liao, Y. Wu, Z. Xu, Y. Zhao, H. Fu, D. Zhang, *Adv. Funct. Mater.* **2012**, *22*, 4862.
[49] H. Luo, S. Chen, Z. Liu, C. Zhang, Z. Cai, X. Chen, G. Zhang, Y. Zhao, S. Decurtins, S.-X. Liu, D. Zhang, *Adv. Funct. Mater.* **2014**, *24*, 4250.
[50] E. Wang, J. W. Y. Lam, R. Hu, C. Zhang, Y. S. Zhao, B. Z. Tang, *J. Mater. Chem. C* **2014**, *2*, 1801.
[51] G. D. Scholes, G. R. Fleming, A. Olaya-Castro, R. van Grondelle, *Nat. Chem.* **2011**, *3*, 763.
[52] J. Iehl, J.-F. Nierengarten, A. Harriman, T. Bura, R. Ziessel, *J. Am. Chem. Soc.* **2012**, *134*, 988.
[53] O. Altan Bozdemir, S. Erbas-Cakmak, O. O. Ekiz, A. Dana, E. U. Akkaya, *Angew. Chemie Int. Ed.* **2011**, *50*, 10907.
[54] N. Karakostas, A. Kaloudi-Chantzea, E. Martinou, K. Seintis, F. Pitterl, H. Oberacher, M. Fakis, J. K. Kallitsis, G. Pistolis, *Faraday Discuss.* **2015**, *185*, 433.
[55] S. Guerra, J. Iehl, M. Holler, M. Peterca, D. a Wilson, B. E. Partridge, S. Zhang, R. Deschenaux, J.-F. Nierengarten, V. Percec, *Chem. Sci.* **2015**, *6*, 3393.
[56] Y.-H. Jeong, M. Son, H. Yoon, P. Kim, D.-H. Lee, D. Kim, W.-D. Jang, *Angew. Chemie Int. Ed.* **2014**, *53*, 6925.
[57] J. ter Schiphorst, A. M. Kendhale, M. G. Debije, C. Menelaou, L. M. Herz, A. P. H. J.

Schenning, *Chem. Mater.* **2014**, *26*, 3876.
[58] G. D. Gutierrez, I. Coropceanu, M. G. Bawendi, T. M. Swager, *Adv. Mater.* **2016**, *28*, 497.
[59] R. Marty, R. Nigon, D. Leite, H. Frauenrath, *J. Am. Chem. Soc.* **2014**, *136*, 3919.
[60] E. R. Draper, J. R. Lee, M. Wallace, F. Jäckel, A. J. Cowan, D. J. Adams, *Chem. Sci.* **2016**, *7*, 6499.
[61] E. R. Draper, T. O. McDonald, D. J. Adams, *Chem. Commun.* **2015**, *51*, 12827.
[62] M. J. Kastelijn, C. W. M. Bastiaansen, M. G. Debije, *Opt. Mater.* **2009**, *31*, 1720.
[63] T. Higashihara, M. Ueda, *Macromolecules* **2015**, *48*, 1915.
[64] V. Fattori, M. Melucci, L. Ferrante, M. Zambianchi, I. Manet, W. Oberhauser, G. Giambastiani, M. Frediani, G. Giachi, N. Camaioni, *Energy Environ. Sci.* **2011**, *4*, 2849.
[65] M. Melucci, M. Durso, L. Favaretto, M. L. Capobianco, V. Benfenati, A. Sagnella, G. Ruani, M. Muccini, R. Zamboni, V. Fattori, N. Camaioni, *RSC Adv.* **2012**, *2*, 8610.
[66] H. Perry, A. Gopinath, D. L. Kaplan, L. Dal Negro, F. G. Omenetto, *Adv. Mater.* **2008**, *20*, 3070.
[67] B. G. Ranby, J. F. Rabek, *Photodegradation, Photo-Oxidation and Photostabilization of Polymers: Principles and Applications*, John Wiley & Sons, Inc., **1975**.
[68] J. W. E. Wiegman, E. van der Kolk, *Sol. Energy Mater. Sol. Cells* **2012**, *103*, 41.
[69] G. Griffini, M. Levi, S. Turri, *Sol. Energy Mater. Sol. Cells* **2013**, *118*, 36.
[70] F. Rey-García, C. Gómez-Reino, M. T. Flores-Arias, G. F. De La Fuente, A. Durán, Y. Castro, *Thin Solid Films* **2011**, *519*, 7982.
[71] S. Parola, B. Julián-López, L. D. Carlos, C. Sanchez, *Adv. Funct. Mater.* **2016**, *26*, 6506.
[72] J. Graffion, A. M. Cojocariu, X. Cattoën, R. A. S. Ferreira, V. R. Fernandes, P. S. André, L. D. Carlos, M. Wong Chi Man, J. R. Bartlett, *J. Mater. Chem.* **2012**, *22*, 13279.
[73] J. Graffion, X. Cattoën, M. Wong Chi Man, V. R. Fernandes, P. S. André, R. A. S. Ferreira, L. D. Carlos, *Chem. Mater.* **2011**, *23*, 4773.
[74] V. T. Freitas, L. Fu, A. M. Cojocariu, X. Cattoën, J. R. Bartlett, R. Le Parc, J.-L. Bantignies, M. Wong Chi Man, P. S. André, R. A. S. Ferreira, L. D. Carlos, *ACS Appl. Mater. Interfaces* **2015**, *7*, 8770.
[75] S. F. H. Correia, P. P. Lima, P. S. André, M. R. S. Ferreira, L. A. D. Carlos, *Sol. Energy Mater. Sol. Cells* **2015**, *138*, 51.
[76] M. M. Nolasco, P. M. Vaz, V. T. Freitas, P. P. Lima, P. S. André, R. A. S. Ferreira, P. D. Vaz, P. Ribeiro-Claro, L. D. Carlos, *J. Mater. Chem. A* **2013**, *1*, 7339.
[77] J. R. Lacowicz, *Principles of Fluorescence Spectroscopy*, Springer Science & Business Media, **2007**.
[78] P. T. M. Albers, C. W. M. Bastiaansen, M. G. Debije, *Sol. Energy* **2013**, *95*, 216.
[79] C. Botta, P. Betti, M. Pasini, *J. Mater. Chem. A* **2013**, *1*, 510.
[80] I. Meazzini, N. Willis-Fox, C. Blayo, J. Arlt, S. Clément, R. C. Evans, *J. Mater. Chem. C* **2016**, *4*, 4049.
[81] P. P. C. Verbunt, A. Kaiser, K. Hermans, C. W. M. Bastiaansen, D. J. Broer, M. G. Debije, *Adv. Funct. Mater.* **2009**, *19*, 2714.
[82] M. G. Debije, *Adv. Funct. Mater.* **2010**, *20*, 1498.
[83] M. G. Debije, C. Menelaou, L. M. Herz, A. P. H. J. Schenning, *Adv. Opt. Mater.* **2014**, *2*, 687.
[84] B. J. Bruijnaers, A. P. H. J. Schenning, M. G. Debije, *Adv. Opt. Mater.* **2015**, *3*, 257.
[85] C. L. Mulder, P. D. Reusswig, A. M. Velázquez, H. Kim, C. Rotschild, M. A. Baldo, *Opt. Express* **2010**, *18*, A79.
[86] A. Jiménez-Solano, J.-M. Delgado-Sánchez, M. E. Calvo, J. M. Miranda-Muñoz, G.

Lozano, D. Sancho, E. Sánchez-Cortezón, H. Míguez, *Prog. Photovoltaics Res. Appl.* **2015**, *23*, 1785.
[87] J. Yoon, L. Li, A. V. Semichaevsky, J. H. Ryu, H. T. Johnson, R. G. Nuzzo, J. A. Rogers, *Nat. Commun.* **2011**, *2*, 343.
[88] M. Peng, S. Hou, H. Wu, Q. Yang, X. Cai, X. Yu, K. Yan, H. Hu, F. Zhu, D. Zou, *J. Mater. Chem. A* **2014**, *2*, 926.
[89] J.-Y. Chen, Y.-C. Chiu, C.-C. Shih, W.-C. Wu, W.-C. Chen, *J. Mater. Chem. A* **2015**, *3*, 15039.
[90] J. C. Goldschmidt, M. Peters, L. Prönneke, L. Steidl, R. Zentel, B. Bläsi, A. Gombert, S. Glunz, G. Willeke, U. Rau, *Phys. Status Solidi Appl. Mater. Sci.* **2008**, *205*, 2811.
[91] A. Bozzola, V. Robbiano, K. Sparnacci, G. Aprile, L. Boarino, A. Proto, R. Fusco, M. Laus, L. C. Andreani, D. Comoretto, *Adv. Opt. Mater.* **2016**, *4*, 147.
[92] G. J. J. Draaisma, D. Reardon, A. P. H. J. Schenning, S. C. J. Meskers, C. W. M. Bastiaansen, *J. Mater. Chem. C* **2016**, *4*, 5747.
[93] I. Levchuk, C. Würth, F. Krause, A. Osvet, M. Batentschuk, U. Resch-Genger, C. Kolbeck, P. Herre, H.-P. Steinrck, W. Peukert, C. J. Brabec, *Energy Environ. Sci.* **2016**, *9*, 1083.
[94] A. Solodovnyk, C. Kick, A. Osvet, H.-J. Egelhaaf, E. Stern, M. Batentschuk, K. Forberich, C. J. Brabec, *Energy Technol.* **2016**, *4*, 385.
[95] D. Alonso-Álvarez, D. Ross, E. Klampaftis, K. R. McIntosh, S. Jia, P. Storiz, T. Stolz, B. S. Richards, *Prog. Photovoltaics Res. Appl.* **2015**, *23*, 479.
[96] T. S. Parel, L. Danos, T. Markvart, *Sol. Energy Mater. Sol. Cells* **2015**, *140*, 306.
[97] Y. H. Ghymn, K. Jung, M. Shin, H. Ko, *Nanoscale* **2015**, *7*, 18642.
[98] S. D. Hodgson, W. S. M. Brooks, A. J. Clayton, G. Kartopu, V. Barrioz, S. J. C. Irvine, *Nano Energy* **2014**, *4*, 1.
[99] M. Hong, T. Xuan, J. Liu, Z. Jiang, Y. Chen, X. Chen, H. Li, *RSC Adv.* **2015**, *5*, 102682.
[100] Y. Li, Z. Li, T. Ablekim, T. Ren, W.-J. Dong, *Phys. Chem. Chem. Phys.* **2014**, *16*, 26193.
[101] W.-B. Hung, T.-M. Chen, *Sol. Energy Mater. Sol. Cells* **2015**, *133*, 39.
[102] T. Fix, A. Nonat, D. Imbert, S. Di Pietro, M. Mazzanti, A. Slaoui, L. J. Charbonnière, *Prog. Photovoltaics Res. Appl.* **2016**, *24*, 1251.
[103] K. Kawano, K. Arai, H. Yamada, N. Hashimoto, R. Nakata, *Sol. Energy Mater. Sol. Cells* **1997**, *48*, 35.
[104] E. Cattaruzza, M. Mardegan, T. Pregnolato, G. Ungaretti, G. Aquilanti, A. Quaranta, G. Battaglin, E. Trave, *Sol. Energy Mater. Sol. Cells* **2014**, *130*, 272.
[105] A. Goetzberger, W. Greube, *Appl. Phys.* **1977**, *14*, 123.
[106] F. Bella, G. Griffini, M. Gerosa, S. Turri, R. Bongiovanni, *J. Power Sources* **2015**, *283*, 195.
[107] S. Marchionna, F. Meinardi, M. Acciarri, S. Binetti, A. Papagni, S. Pizzini, V. Malatesta, R. Tubino, *J. Lumin.* **2006**, *118*, 325.
[108] T. Maruyama, A. Enomoto, K. Shirasawa, *Sol. Energy Mater. Sol. Cells* **2000**, *64*, 269.
[109] B. S. Richards, K. R. McIntosh, *Prog. Photovoltaics Res. Appl.* **2007**, *15*, 27.
[110] K. Machida, H. Li, D. Ueda, S. Inoue, G. Adachi, *J. Lumin.* **2000**, *87–89*, 1257.
[111] D. Pintossi, G. Iannaccone, A. Colombo, F. Bella, M. Välimäki, K.-L. Väisänen, J. Hast, M. Levi, C. Gerbaldi, C. Dragonetti, S. Turri, G. Griffini, *Adv. Electron. Mater.* **2016**, *2*, 1600288.
[112] T.-T. Xuan, J.-Q. Liu, H.-L. Li, H.-C. Sun, L. Pan, X.-H. Chen, Z. Sun, *RSC Adv.* **2015**, *5*, 7673.
[113] V. Švrček, A. Slaoui, J.-C. Muller, *Thin Solid Films* **2004**, *451*, 384.
[114] H.-V. Han, C.-C. Lin, Y.-L. Tsai, H.-C. Chen, K.-J. Chen, Y.-L. Yeh, W.-Y. Lin, H.-C.

Kuo, P. Yu, *Sci. Rep.* **2014**, *4*, 5734.
[115] G. C. Glaeser, U. Rau, *Thin Solid Films* **2007**, *515*, 5964.
[116] "Solar PV Market Share by Cell Technology," can be found under https://www.statista.com/statistics/492724/solar-pv-global-market-share-by-cell-technology/, **2016**
[117] C. P. Thomas, A. B. Wedding, S. O. Martin, *Sol. Energy Mater. Sol. Cells* **2012**, *98*, 455.
[118] C. Strümpel, M. McCann, G. Beaucarne, V. Arkhipov, A. Slaoui, V. Švrček, C. del Cañizo, I. Tobias, *Sol. Energy Mater. Sol. Cells* **2007**, *91*, 238.
[119] L. D. Carlos, R. A. S. Ferreira, V. de Z. Bermudez, S. J. L. Ribeiro, *Adv. Mater.* **2009**, *21*, 509.
[120] J. Y. Chen, C. K. Huang, W. B. Hung, K. W. Sun, T. M. Chen, *Sol. Energy Mater. Sol. Cells* **2014**, *120*, 168.
[121] S. Kalytchuk, S. Gupta, O. Zhovtiuk, A. Vaneski, S. V. Kershaw, H. Fu, Z. Fan, E. C. H. Kwok, C.-F. Wang, W. Y. Teoh, A. L. Rogach, *J. Phys. Chem. C* **2014**, *118*, 16393.
[122] J. Xu, S. Sun, Y. Cao, P. Lu, W. Li, K. Chen, *Part. Part. Syst. Charact.* **2014**, *31*, 459.
[123] M. Brossard, C.-Y. Hong, M. Hung, P. Yu, M. D. B. Charlton, P. G. Savvidis, P. G. Lagoudakis, *Adv. Opt. Mater.* **2015**, *3*, 263.
[124] Y.-K. Liao, M. Brossard, D.-H. Hsieh, T.-N. Lin, M. D. B. Charlton, S.-J. Cheng, C.-H. Chen, J.-L. Shen, L.-T. Cheng, T.-P. Hsieh, F.-I. Lai, S.-Y. Kuo, H.-C. Kuo, P. G. Savvidis, P. G. Lagoudakis, *Adv. Energy Mater.* **2015**, *5*, 1401280.
[125] K. Bouras, G. Schmerber, H. Rinnert, D. Aureau, H. Park, G. Ferblantier, S. Colis, T. Fix, C. Park, W. K. Kim, A. Dinia, *Sol. Energy Mater. Sol. Cells* **2016**, *145*, 134.
[126] Y. Li, Z. Li, Y. Wang, A. Compaan, T. Ren, W.-J. Dong, *Energy Environ. Sci.* **2013**, *6*, 2907.
[127] J. Liu, Q. Yao, Y. Li, *Appl. Phys. Lett.* **2006**, *88*, 173119.
[128] G. Griffini, F. Bella, F. Nisic, C. Dragonetti, D. Roberto, M. Levi, R. Bongiovanni, S. Turri, *Adv. Energy Mater.* **2015**, *5*, 1401312.
[129] H. Ahmed, J. Doran, S. J. McCormack, *Sol. Energy* **2016**, *126*, 146.
[130] Z. Hosseini, W. K. Huang, C. M. Tsai, T. M. Chen, N. Taghavinia, E. W. G. Diau, *ACS Appl. Mater. Interfaces* **2013**, *5*, 5397.
[131] M. Jørgensen, K. Norrman, S. A. Gevorgyan, T. Tromholt, B. Andreasen, F. C. Krebs, *Adv. Mater.* **2012**, *24*, 580.
[132] W. Xu, H. Song, D. Yan, H. Zhu, Y. Wang, S. Xu, X. Bai, B. Dong, Y. Liu, *J. Mater. Chem.* **2011**, *21*, 12331.
[133] J. Kettle, N. Bristow, D. T. Gethin, Z. Tehrani, O. Moudam, B. Li, E. A. Katz, G. A. dos Reis Benatto, F. C. Krebs, *Sol. Energy Mater. Sol. Cells* **2016**, *144*, 481.
[134] O. Moudam, N. Bristow, S.-W. Chang, M. Horie, J. Kettle, *RSC Adv.* **2015**, *5*, 12397.
[135] J. J. Huang, Z. F. Zhong, M. Z. Rong, X. Zhou, X. D. Chen, M. Q. Zhang, *Carbon* **2014**, *70*, 190.
[136] G. F. Ma, H. J. Xie, P. P. Cheng, Y. Q. Li, J. X. Tang, *Appl. Phys. Lett.* **2013**, *103*, 43302.
[137] M. Prosa, A. Sagnella, T. Posati, M. Tessarolo, M. Bolognesi, S. Cavallini, S. Toffanin, V. Benfenati, M. Seri, G. Ruani, M. Muccini, R. Zamboni, *RSC Adv.* **2014**, *4*, 44815.
[138] D. Bi, C. Yi, J. Luo, J.-D. Décoppet, F. Zhang, S. M. Zakeeruddin, X. Li, A. Hagfeldt, M. Grätzel, *Nat. Energy* **2016**, *1*, 16142.
[139] T. A. Berhe, W.-N. Su, C.-H. Chen, C.-J. Pan, J.-H. Cheng, H.-M. Chen, M.-C. Tsai, L.-Y. Chen, A. A. Dubale, B.-J. Hwang, *Energy Environ. Sci.* **2016**, *9*, 323.
[140] N. Chander, A. F. Khan, P. S. Chandrasekhar, E. Thouti, S. K. Swami, V. Dutta, V. K. Komarala, *Appl. Phys. Lett.* **2014**, *105*, 33904.
[141] X. Hou, T. Xuan, H. Sun, X. Chen, H. Li, L. Pan, *Sol. Energy Mater. Sol. Cells* **2016**,

149, 121.
[142] F. Bella, G. Griffini, J.-P. Correa-Baena, G. Saracco, M. Grätzel, A. Hagfeldt, S. Turri, C. Gerbaldi, *Science* **2016**, *354*, 203.
[143] M.-F. Joubert, *Opt. Mater.* **1999**, *11*, 181.
[144] F. Wang, R. Deng, J. Wang, Q. Wang, Y. Han, H. Zhu, X. Chen, X. Liu, *Nat. Mater.* **2011**, *10*, 968.
[145] N. Yanai, N. Kimizuka, *Chem. Commun.* **2016**, *52*, 5354.
[146] C. Ye, L. Zhou, X. Wang, Z. Liang, *Phys. Chem. Chem. Phys.* **2016**, *18*, 10818.
[147] S. Wu, X. Sun, J. Zhu, J. Chang, S. Zhang, *Nanotechnology* **2016**, *27*, 345703.
[148] X. Chen, W. Xu, H. Song, C. Chen, H. Xia, Y. Zhu, D. Zhou, S. Cui, Q. Dai, J. Zhang, *ACS Appl. Mater. Interfaces* **2016**, *8*, 9071.
[149] S. Fischer, R. Martín-Rodríguez, B. Fröhlich, K. W. Krämer, A. Meijerink, J. C. Goldschmidt, *J. Lumin.* **2014**, *153*, 281.
[150] M. Pokhrel, G. A. Kumar, D. K. Sardar, *J. Mater. Chem. A* **2013**, *1*, 11595.
[151] M. Haase, H. Schäfer, *Angew. Chemie Int. Ed.* **2011**, *50*, 5808.
[152] J. Bai, R. Zhao, G. Han, Z. Li, G. Diao, *RSC Adv.* **2015**, *5*, 43328.
[153] N. Chander, A. F. Khan, V. K. Komarala, S. Chawla, V. Dutta, *Prog. Photovoltaics Res. Appl.* **2016**, *24*, 692.
[154] P. Du, J. H. Lim, S. H. Kim, J. S. Yu, *Opt. Mater. Express* **2016**, *6*, 3839.
[155] J. Yu, Y. Yang, R. Fan, P. Wang, Y. Dong, *Nanoscale* **2016**, *8*, 4173.
[156] M. He, X. Pang, X. Liu, B. Jiang, Y. He, H. Snaith, Z. Lin, *Angew. Chemie Int. Ed.* **2016**, *55*, 4280.
[157] J. Roh, H. Yu, J. Jang, *ACS Appl. Mater. Interfaces* **2016**, *8*, 19847.
[158] H. Wang, X. Hong, R. Han, J. Shi, Z. Liu, S. Liu, Y. Wang, Y. Gan, *Sci. Rep.* **2015**, *5*, 17088.
[159] W. Shao, G. Chen, T. Y. Ohulchanskyy, A. Kuzmin, J. Damasco, H. Qiu, C. Yang, H. Ågren, P. N. Prasad, *Adv. Opt. Mater.* **2015**, *3*, 575.
[160] M. D. Wisser, S. Fischer, P. C. Maurer, N. D. Bronstein, S. Chu, A. P. Alivisatos, A. Salleo, J. A. Dionne, *ACS Photonics* **2016**, *3*, 1523.
[161] G. Chen, J. Damasco, H. Qiu, W. Shao, T. Y. Ohulchanskyy, R. R. Valiev, X. Wu, G. Han, Y. Wang, C. Yang, H. Ågren, P. N. Prasad, *Nano Lett.* **2015**, *15*, 7400.
[162] T. N. Singh-Rachford, J. Lott, C. Weder, F. N. Castellano, *J. Am. Chem. Soc.* **2009**, *131*, 12007.
[163] A. Monguzzi, M. Mauri, A. Bianchi, M. K. Dibbanti, R. Simonutti, F. Meinardi, *J. Phys. Chem. C* **2016**, *120*, 2609.
[164] P. E. Keivanidis, S. Baluschev, T. Miteva, G. Nelles, U. Scherf, A. Yasuda, G. Wegner, *Adv. Mater.* **2003**, *15*, 2095.
[165] P. Duan, N. Yanai, H. Nagatomi, N. Kimizuka, *J. Am. Chem. Soc.* **2015**, *137*, 1887.
[166] K. Sripathy, R. W. MacQueen, J. R. Peterson, Y. Y. Cheng, M. Dvořák, D. R. McCamey, N. D. Treat, N. Stingelin, T. W. Schmidt, *J. Mater. Chem. C* **2015**, *3*, 616.
[167] A. Nattestad, Y. Y. Cheng, R. W. MacQueen, T. F. Schulze, F. W. Thompson, A. J. Mozer, B. Fückel, T. Khoury, M. J. Crossley, K. Lips, G. G. Wallace, T. W. Schmidt, *J. Phys. Chem. Lett.* **2013**, *4*, 2073.
[168] T. F. Schulze, J. Czolk, Y.-Y. Cheng, B. Fückel, R. W. MacQueen, T. Khoury, M. J. Crossley, B. Stannowski, K. Lips, U. Lemmer, A. Colsmann, T. W. Schmidt, *J. Phys. Chem. C* **2012**, *116*, 22794.
[169] Y. Y. Cheng, B. Fückel, R. W. MacQueen, T. Khoury, R. G. C. R. Clady, T. F. Schulze, N. J. Ekins-Daukes, M. J. Crossley, B. Stannowski, K. Lips, T. W. Schmidt, *Energy Environ. Sci.* **2012**, *5*, 6953.
[170] Y. Y. Cheng, A. Nattestad, T. F. Schulze, R. W. MacQueen, B. Fückel, K. Lips, G. G. Wallace, T. Khoury, M. J. Crossley, T. W. Schmidt, *Chem. Sci.* **2015**, *7*, 559.

[171] M. Wu, D. N. Congreve, M. W. B. Wilson, J. Jean, N. Geva, M. Welborn, T. Van Voorhis, V. Bulovi, M. G. Bawendi, M. A. Baldo, *Nat. Photonics* **2015**, *10*, 31.
[172] K. Börjesson, P. Rudquist, V. Gray, K. Moth-Poulsen, *Nat. Commun.* **2016**, *7*, 12689.
[173] Z. Huang, X. Li, B. D. Yip, J. M. Rubalcava, C. J. Bardeen, M. L. Tang, *Chem. Mater.* **2015**, *27*, 7503.
[174] J. Zimmermann, R. Mulet, G. D. Scholes, T. Wellens, A. Buchleitner, *J. Chem. Phys.* **2014**, *141*, 184104.
[175] X. Yu, X. Cao, X. Chen, N. Ayres, P. Zhang, *Chem. Commun. (Camb).* **2015**, *51*, 588.
[176] A. L. Hagstrom, F. Deng, J.-H. Kim, *ACS Photonics* **2017**, *4*, 127.
[177] F. M. Vossen, M. P. J. Aarts, M. G. Debije, *Energy Build.* **2016**, *113*, 123.
[178] T. Trupke, M. A. Green, P. Würfel, *J. Appl. Phys.* **2002**, *92*, 1668.
[179] O. M. Ten Kate, M. De Jong, H. T. Hintzen, E. Van Der Kolk, *J. Appl. Phys.* **2013**, *114*, 84502.
[180] J. J. Eilers, D. Biner, J. T. van Wijngaarden, K. Krämer, H.-U. Güdel, A. Meijerink, *Appl. Phys. Lett.* **2010**, *96*, 151106.
[181] L. de A. Florêncio, L. A. Gómez-Malagón, B. C. Lima, A. S. L. Gomes, J. A. M. Garcia, L. R. P. Kassab, *Sol. Energy Mater. Sol. Cells* **2016**, *157*, 468.
[182] M. C. Beard, A. G. Midgett, M. C. Hanna, J. M. Luther, B. K. Hughes, A. J. Nozik, *Nano Lett.* **2010**, *10*, 3019.
[183] D. Timmerman, I. Izeddin, P. Stallinga, I. N. Yassievich, T. Gregorkiewicz, *Nat. Photonics* **2008**, *2*, 105.
[184] D. Timmerman, J. Valenta, K. Dohnalová, W. D. A. M. de Boer, T. Gregorkiewicz, *Nat. Nanotechnol.* **2011**, *6*, 710.